Jamile Katiele Fritzen

The impact of axion emission on the cooling of white dwarf stars

Brasil

01/08/2021

Jamile Katiele Fritzen

The impact of axion emission on the cooling of white dwarf stars

Dissertação submetida ao Programa de Pós Graduação em Física do Instituto de Física da UFRGS, como quesito parcial para obtenção do título de Mestre em Física, com ênfase em Astronomia.

Universidade Federal do Rio Grande do Sul – UFRGS

Instituto de Física

Programa de Pós-Graduação

Supervisor: Alejandra Daniela Romero

Co-supervisor: Kepler de Souza Oliveira Filho

Brasil

01/08/2021

Jamile Katiele Fritzen
The impact of axion emission on the cooling of white dwarf stars/ Jamile Katiele Fritzen. – Brasil, 01/08/2021-
78 p. : il. (algumas color.) ; 30 cm.

Supervisor: Alejandra Daniela Romero

Master Thesis – Universidade Federal do Rio Grande do Sul – UFRGS
Instituto de Física
Programa de Pós-Graduação, 01/08/2021.

1. White dwarfs. 2. Axions. I. Supervisor Alejandra Romero. II. UFRGS. III. Instituto de Física. IV. The impact of axion emission on the cooling of white dwarf stars

CDU 02:141:005.7

Jamile Katiele Fritzen

The impact of axion emission on the cooling of white dwarf stars

Dissertação submetida ao Programa de Pós Graduação em Física do Instituto de Física da UFRGS, como quesito parcial para obtenção do título de Mestre em Física, com ênfase em Astronomia.

Trabalho aprovado. Brasil, 27 de agosto de 2021:

Alejandra Daniela Romero
Orientadora

Kepler de Souza Oliveira Filho
Coorientador

Marcos Perez Diaz
Convidado

Farinaldo Queiroz
Convidado

Marina Trevisan
Convidada

Brasil
01/08/2021

To anyone curious about the universe, in particular to the ones who made from this curiosity their career and resist despite all the odds.

Acknowledgements

I would like to thank a number of people, without whom I would not have been able to complete this research.

First of all, I would like to express my sincere gratitude to my boyfriend. The pandemic made everything more difficult, but having you on my side (literally) everyday made it a lot easier.

I obviously can't help but say thanks to my mom, who is always supporting and encouraging me. Thank you for always letting me follow my dreams.

A big thanks to my sister, who inspired and encouraged me.

I also want to thank my friends for always being there for me. Here I have the obligation to mention Larissa and Theylor, who helped me in the research and also helped me to deal with frustrations and pressure along the research.

I am also grateful to the AstroUFRGS members, who embraced with me the aim to communicate the science outside academia.

I cannot leave my supervisors, Alejandra and Kepler, without mentioning, who trusted me as a scientist more than me. Thank you for your patience, explanations and corrections.

Finally, this thesis would not be possible without the financial support of CAPES.

"Look again at that dot. That's here. That's home. That's us. On it everyone you love, everyone you know, everyone you ever heard of, every human being who ever was, lived out their lives. The aggregate of our joy and suffering, thousands of confident religions, ideologies, and economic doctrines, every hunter and forager, every hero and coward, every creator and destroyer of civilization, every king and peasant, every young couple in love, every mother and father, hopeful child, inventor and explorer, every teacher of morals, every corrupt politician, every "superstar," every "supreme leader," every saint and sinner in the history of our species lived there–on a mote of dust suspended in a sunbeam.

The Earth is a very small stage in a vast cosmic arena. Think of the rivers of blood spilled by all those generals and emperors so that, in glory and triumph, they could become the momentary masters of a fraction of a dot. Think of the endless cruelties visited by the inhabitants of one corner of this pixel on the scarcely distinguishable inhabitants of some other corner, how frequent their misunderstandings, how eager they are to kill one another, how fervent their hatreds.

Our posturings, our imagined self-importance, the delusion that we have some privileged position in the Universe, are challenged by this point of pale light. Our planet is a lonely speck in the great enveloping cosmic dark. In our obscurity, in all this vastness, there is no hint that help will come from elsewhere to save us from ourselves."

- Carl Sagan, Pale Blue Dot, 1994

Abstract

Axions are theoretical particles that have been probed in stellar systems such as white dwarf stars, which have already been shown to be excellent laboratories for the study of axions with coupling to electrons. However, there has been little discussion about the impact these particles can have on the cooling time of white dwarf stars. In this work I investigate the impact of axion emission on white dwarf stars of different metallicities, focusing on their cooling times. Using the La Plata evolutionary code to calculate consistent models, I computed white dwarf cooling sequences considering metallicities Z=0.01, 0.004 and 0.0001, white dwarf masses $0.524M_{\odot} < M_{WD} < 0.917M_{\odot}$ and axions with masses from 1 to 30 meV, equivalent to an axion to electron coupling coefficient $2.8 \times 10^{-14} \leq g_{ae} \leq 8.4 \times 10^{-13}$. I found that the cooling rate of the white dwarfs is strongly affected by the presence of axions, and the cooling times can be reduced up to 5 Gyrs for $T_{\rm eff} \lesssim 5000$K - independent of the metallicity. I propose the usage of the white dwarf cooling sequence of globular clusters as a new method to constrain the axion mass. I determined ages for 47 Tucanae using isochrones obtained with models without axions and including axions of 17 and 30meV, which resulted in an age difference of 2.1 and 4.2 Gyr, respectively. Comparing it to independent age determinations I was able to constrain the axion mass to $m_a < 17$ meV ($g_{ae} < 4.8 \times 10^{-13}$).

Key words: white dwarfs. axions. dark matter.

Resumo

Os áxions são partículas teóricas que têm sido testados em sistemas estelares como anãs brancas, que já se mostraram excelentes laboratórios para o estudo de áxions que interagem com elétrons. No entanto, há pouca discussão sobre o impacto que essas partículas podem ter no tempo de resfriamento de estrelas anãs brancas. Neste trabalho, investigamos o impacto de emissão de áxions em estrelas anãs brancas de diferentes metalicidades, com foco em seus tempos de resfriamento. Usando o código de La Plata (LPCODE) para obter modelos consistentes, calculei o resfriamento de sequências de anãs brancas considerando metalicidades $Z = 0,01$, $0,004$ e $0,0001$, massas de anã branca $0,524M_{\odot} < M_{WD} < 0,917M_{\odot}$ e massas de áxions de 1 a 30 meV ($2,8 \times 10^{-14} \leq g_{ae} \leq 8,4 \times 10^{-13}$). Descobri que a taxa de resfriamento das anãs brancas é bastante afetada pela presença de áxions, e os tempos de resfriamento podem ser reduzidos em até 5 Gyrs para $T_{\rm eff} \lesssim 5\,000K$ - independente da metalicidade. Adicionalmente, proponho o uso da sequência de resfriamento de anãs brancas de aglomerados globulares como um novo método para restringir a massa do áxion. Determinei idades para 47 Tucanae usando isócronas obtidas com modelos sem áxions e incluindo axions de 17 e 30 meV, o que resultou em uma diferença de idade de 2,1 e 4,2 Gyrs, respectivamente. Comparando com determinações independentes de idade pude restringir a massa do áxion a $m_a \leq 17$ meV ($g_{ae} < 4,8 \times 10^{-13}$).

Palavras-chave: Anãs brancas. áxions. matéria escura.

Press Release

Um passo na busca pela matéria escura do Universo

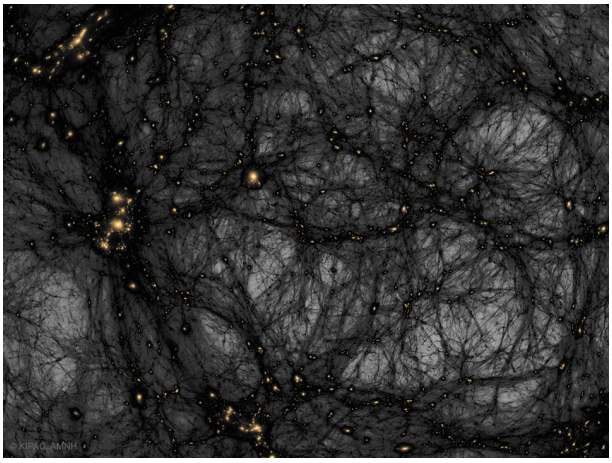

Figure 1 – Matéria escura (em preto) num universo simulado. Fonte: APOD

Apesar de todas as descobertas na Astronomia nos últimos anos, a composição de mais de 80% da massa do Universo permanece um mistério. É a chamada Matéria Escura, e descobrir do que ela é feita é uma das principais questões em aberto na Astrofísica atual. No meu trabalho de mestrado eu estudei um dos principais candidatos a compor a matéria escura: o áxion. Apesar de o áxion não interagir com quase nada, descobri que dependendo da sua massa ele pode causar efeitos notáveis na evolução de certas estrelas.

A existência do áxion foi proposta em 1977 e até hoje não foi confirmada. Sua massa e algumas outras características não são bem definidas pela teoria, tornando-o ainda mais difícil de ser encontrado. A existência de certos comportamentos observados em estrelas podem, no entanto, nos trazer pistas da existência (ou não) dessa partícula.

Foi pensando nisso que eu, sob orientação de Alejandra Romero e Kepler de Oliveira, comecei a simular o comportamento de estrelas anãs brancas com a inclusão de áxions. Essas estrelas são o que restam depois que estrelas como o Sol morrem, e em geral é possível descrever com muita precisão seu comportamento. Com essas simulações percebi que o áxion pode aumentar muito a velocidade de envelhecimento dessas estrelas, dependendo de sua massa. Comparando as idades que obtive em minhas simulações com idades determinadas de formas independentes, concluí que o áxion deve ser extremamtente leve, cerca de 3 000 000× mais leve que o elétron!

Pesquisas como essa dão suporte para outros pesquisadores, que buscam observar a matéria escura: “É muito mais fácil encontrar algo quando sabemos o que estamos procurando”. Por isso, esse é um passo importante para desvendar do que é feita a maior parte do nosso Universo.

Palavras-chave: Anãs brancas. áxions. matéria escura.

List of Figures

List of Tables

List of abbreviations and acronyms

AGB	Assymptotic Gyant Branch
BBN	Big Bang nucleosynthesis
C	Carbon
Λ CDM	Lambda-Cold Dark Matter model
CMB	Cosmic Microwave Background
CMD	Color-Magnitude diagram
CP problem	Charge-Parity problem
H	Hydrogen
He	Helium
IFMR	Initial-to-final mass relation
IMF	Initial Mass Function
MACHOs	Massive Compact Objects
O	Oxygen
WD	White Dwarf
WIMPs	Weak Interactive Massive Particles

List of symbols

g_{ae}	axion coupling to electrons
$g_{a\gamma\gamma}$	axion coupling to photons
$L_{\odot}$	Solar luminosity
$M_{\odot}$	Solar mass
m_a	axion mass
T_{eff}	Effective temperature
Z	metallicity

Contents

1 Introduction

1.1 Stellar evolution[1]

The stars are luminous spheroids of plasma held together by their gravity, whose existence relies on a delicate equilibrium of forces. As sometimes the equilibrium is temporarily broken, the stars happen to perceptively change over time. The compilation of these changes designates what is called stellar evolution.

The properties of a star, its lifetime, and how it evolve depend mainly on only three properties: its initial mass, the abundance of metals in it (metallicity), and if the star is alone or interacting with other stars. For simplicity, in this work only the evolution of single stars will be presented. In general, the lower is the mass of the star, the longer it will shine. There is, though, a minimum mass for the star to reach stable nuclear reactions to maintain its equilibrium and luminosity. Objects with a mass lower than $\sim 0.08 M_\odot$ get degenerate before the ignition of hydrogen and become brown dwarfs.

The process to form a star begins when a molecular cloud becomes gravitationally unstable due to a perturbation. It contracts and fragments itself, giving rise to many objects. The contraction of each cloud releases thermal energy, heating up the central region. When the central region of a fragment of the cloud reaches the temperature of $\sim 6 \times 10^6$ K, the hydrogen burning takes place in the central regions, stopping the contraction and establishing the beginning of the main sequence.

The main sequence is the longest stage in the star lifetime. During this phase, the star obtains energy through the conversion of hydrogen nucleus into helium in the core. The conversion can occur via two main processes: the proton-proton chain and the CNO cycle. The first process dominates for stars with $M \lesssim 1.75 M_\odot$ and the second for stars with masses higher than $\sim 1.75 M_\odot$. The efficiency of the two processes depends strongly on the central temperature of the star. As the more massive ones have higher temperatures (and consequently higher luminosity), the hydrogen is consumed sooner for those stars. The typical temporal scale on the main sequence is, therefore, higher for lower mass stars (e. g. $\sim 10^{10}$ yr for $1 M_\odot$) and lower for the higher mass stars (e. g. $\sim 10^9$ yr for $2 M_\odot$).

During the main sequence, the star stays in hydrodynamical equilibrium, i.e. balance between the gravitational force and the pressure of the gas. The pressure of the gas is sustained by the thermonuclear reactions inside the star. When the star consumes $\sim 10\%$ of its hydrogen content, the center of the star begins to be occupied only by the helium

[1] Section based on the book “Stellar Structure and Evolution”, Kippenhahn, Rudolf; Weigert, Alfred; Weiss, Achim, 2012 [5]

nucleus and the equilibrium is affected. When that happens, the main sequence stage reaches its end. At this point, the star will be left with a He core, a layer of H burning and an envelope of H.

The post main sequence evolution will significantly depend on the initial mass of the star. Stars with masses lower than $\sim 0.45 M_{\odot}$ will never reach the temperature to the helium burning in their core and will end their lives as white dwarfs with helium core.

When stars with masses higher than $\sim 0.45 M_{\odot}$ leave the main sequence, the helium core starts to contract, releasing thermal energy. This energy then heats up the upper layers. As the hydrogen burning is still happening in a layer above the helium core, the efficiency of the hydrogen burning increases, increasing the star's luminosity. The outer regions then expand and its superficial temperature drops. At this point the star becomes a red giant. The He burning, however, starts through different process, depending on the mass of the star.

In stars with masses between $\sim 0.45 M_{\odot}$ and $\sim 2 M_{\odot}$, electron degeneracy takes place in the contracting helium core, and the degeneracy pressure interrupts the contraction. In this new equilibrium state, the hydrogen burning layer keeps increasing the mass of the helium core, which slowly shrinks. As the core is degenerate, the helium burning starts drastically when it reaches its burning temperature ($\sim 10^8$ K). This episode is called helium flash.

For stars with masses higher than $\sim 2 M_{\odot}$, the helium burning takes place more mildly. The helium core contracts until the temperature for the helium burning is reached. When the helium burning starts, the core stops to contract and a new equilibrium is achieved.

Helium burning occurs similarly for all stars. At the beginning of the burning, three helium nuclei combine into one carbon nucleus. As the amount of carbon grows, oxygen is also produced. This phase lasts for approximately 10% of the main sequence duration. When the central helium is consumed, the star gets unstable again.

In general, stars with masses between $\sim 0.45 M_{\odot}$ and $\sim 10 M_{\odot}$ do not reach the necessary conditions for carbon and oxygen burning. After the central helium is consumed, the carbon/oxygen core contracts and soon gets degenerated. As thermal energy is released in the process, the upper layers get hotter and expand. The star enters then in the AGB (asymptotic giant branch) phase. During this phase, the star has two burning regions: the helium burning layer and the hydrogen burning layer. At some point, the helium layer gets too thin and becomes unstable, starting a thermal pulse. The outer layers then expand and the hydrogen burning layer becomes inactive. The star then contracts and the hydrogen layer gets active again. The instability on the helium layer can happen again, and more thermal pulses can occur. At each thermal pulse the star loses the outer parts as a result

of its expansion. Once the mass of the envelope is reduced, the thermal pulses stop. After the star ejects the outer layers, what is left is a white dwarf star.

Stars with masses higher than $\sim 10M_{\odot}$ will continue to burn heavier elements in their cores until iron is formed. Iron is the chemical element with the highest binding energy, and its fusion consumes energy instead of releasing it. The iron core violently explodes in an event called Supernova. If the star has an initial mass of less than $\sim 25M_{\odot}$, the object that is left is a neutron star; if the initial mass of the star is greater than $\sim 25M_{\odot}$, the star will end as a black hole.

The evolution of a single star can be visualized in an HR diagram, which shows the relation between temperature and luminosity of a star. In Figure 2 I present the path of a modeled star with $1M_{\odot}$ and solar metallicity in the HR diagram throughout its evolution. Each phase that the star pass through is marked with a different color.

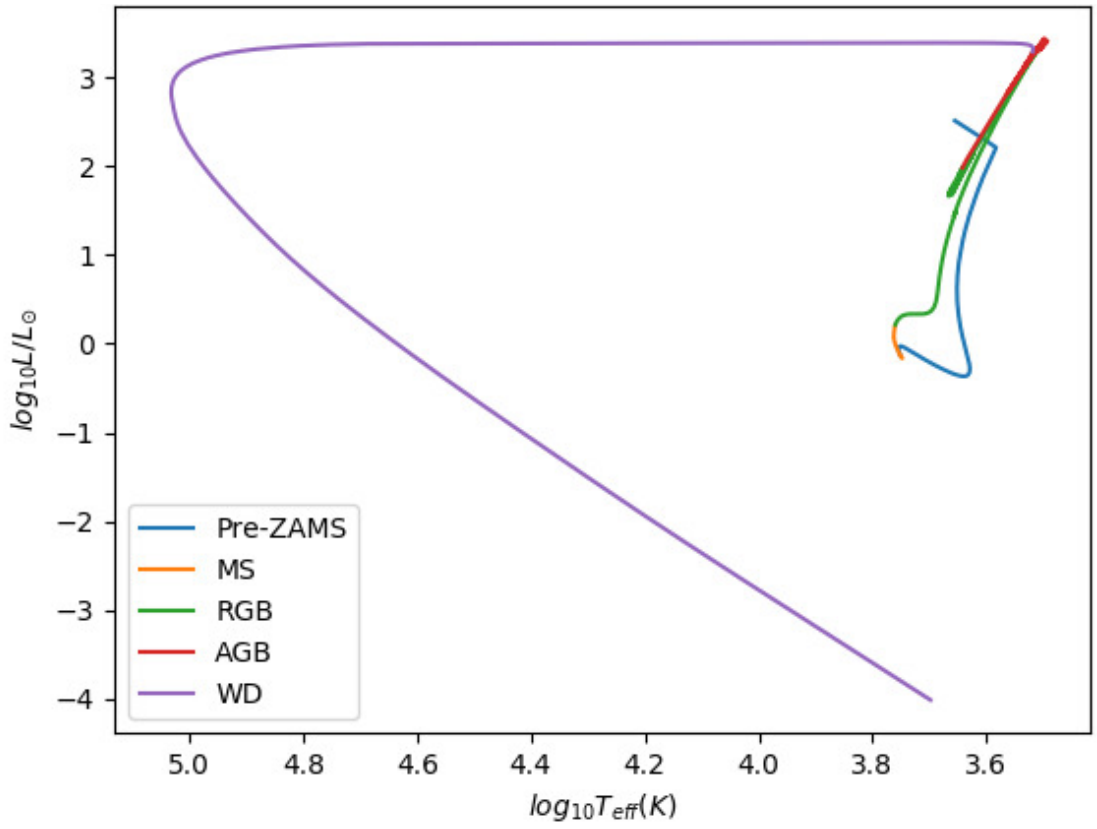

Figure 2 – HR diagram in which it is shown the evolution of a single $1M_{\odot}$, $Z = 0.02$ star. In blue it is shown the path of a forming star, in orange the main-sequence phase, in green the red-giant branch (RGB), in red the asymptotic giant-branch (AGB) and in purple it is shown the formation and cooling of a white dwarf.

1.2 White Dwarf stars[2]

The first white dwarf star was reported in 1914 [7]. At that time, 40 Eridani B caught the attention of astronomers for being placed below the main sequence in the HR diagram, which means a very small radius. The afterward observation of the same characteristics in Sirius B [8] pointed to a new class of stars. As the mass of Sirius B was known, the determination of its mean density was possible and its value turned out to be impressively high. Such high densities could not be explained at that time, and only with the advent of quantum mechanics a better understanding of these stars emerged [9].

Unlike main sequence stars, the white dwarf stars are not supported against gravity by the pressure generated by the nuclear reactions. These stars are in a such dense state that the electron gas is degenerated, i.e. the lowest energy states for the electrons in the gas are occupied. The electrons are forced to occupy higher momentum states, which generate the pressure that supports the star against gravity:

$$P_{e,nr} = \frac{h^2}{20 m_e} \left(\frac{3}{\pi}\right)^{\frac{2}{3}} n_e^{\frac{5}{3}}, \tag{1.1}$$

in which h is the Plank constant, m_e is the electron mass and n_e is the electron density. The electron degeneracy pressure does not depend on the temperature, so a decrease in the gas temperature does not mean a reduction of the pressure. It means that, in general, the mechanical and thermal structures can be treated separately. The degeneracy is also responsible for their unusual property to have their size inversely proportional to their mass. Using the equation 1.1 on the equation of the hydrostatic equilibrium it is possible to see that the mass is

$$M \propto R^{-3}, \tag{1.2}$$

in which R is the radius of the star.

The gas, however, cannot be indefinitely dense. As the density grows, the electrons are forced to occupy higher and higher momentum states, until the relativistic limit is reached. The maximum mass the star can have is called Chandrasekhar mass, and it can be derived by using the relativistic version of equation 1.1 into the hydrostatic equilibrium equation. It is given by

$$M_{Ch} = \frac{5.826}{\mu_e^2 M_\odot}, \tag{1.3}$$

[2]Section based on the review "Evolutionary and pulsational properties of white dwarf stars", Leandro G. Althaus, Alejandro H. Corsico, Jordi Isern, Enrique Garcıa–Berro, 2010 [6]

in which μ_e is the average molecular weight per electron. For larger masses the electron degeneracy pressure cannot hold the gravitational collapse, and no stable white dwarf can exist.

The white dwarf stars are now established as being the end product of the evolution of low and intermediate-mass stars (up to $5 - 12 M_\odot$ [10], depending on their initial metallicity). Although a white dwarf star cannot exceed the Chandrasekhar mass, its progenitor can have larger masses due to the intense mass loss during its evolution, mainly during the AGB phase.

It is observed that lower-mass stars are formed in a greater quantity compared to more massive ones. The probability of a star to be formed within a certain range of mass can be determined using an initial mass function (IMF). Using the Salpeter distribution ($\xi \propto M^{-2.35}$) [11], we can estimate the fraction of stars formed that will turn into white dwarfs:

$$\int_{0.08}^{10} 0.04462 M^{-2.35} dM = 0.9986. \tag{1.4}$$

Hence almost all stars will turn into white dwarfs eventually. The white dwarfs are, therefore, the most common end product of stars.

A white dwarf star is formed after the star passes through the AGB phase and expels its outer layers in a planetary nebula. The remnant core is at high temperatures ($T_{\text{eff}} \approx 100\,000$K), but has no appreciable sources of nuclear energy. During the early stages of the white dwarf cooling nuclear fusion is still happening in the upper layers. Although the CNO reactions can contribute to the luminosity of the white dwarf at the early stages, these stages do not last for sufficient time for the reactions to be important on the white dwarfs cooling times. It can impact, however, the thickness of the hydrogen envelope of the white dwarfs.

Most of the formed white dwarf stars hold a core made of carbon and oxygen, surrounded by a thin helium layer, which is surrounded by a thin hydrogen layer. Despite the lack of nuclear fusion in its core, the star keeps shining for a long time by converting the internal energy into radiation. Its temperature, therefore, slowly decreases with time, as well as its luminosity. Additional sources and sinks of energy can, however, impact the cooling times of white dwarfs.

The cooling of a white dwarf star occurs not only by photon emission but also by neutrino emission. Neutrinos are created in the inner part of the white dwarfs, mainly via the plasma-neutrino process and bremsstrahlung process [12]. As these particles have a small cross-section, they can freely escape from the star, carrying energy away. For young white dwarfs, the neutrinos can represent the major energy-loss mechanism [13].

As the white dwarfs cool down, the electrostatic interactions become important, and at some point, the thermal motions are no longer sufficient to prevent the ions from

reorganizing themselves in a lattice structure [14]. The center of the star will then begin to freeze into a crystalline solid, releasing latent energy and consequently slowing the cooling rate. It happens when

$$\Gamma = \frac{1}{kT}\frac{(Ze)^2}{R} >> 1, \tag{1.5}$$

in which k is the Boltzmann constant, Z is the atomic number, e is the electron charge and R is the inter-ionic separation.

At approximately the same effective temperature at which the crystallization takes place, the external convection zone of the white dwarfs reaches the degenerate core, in an event called convective coupling. As the convection is more efficient than the radiation at transporting energy, the energy of the core will be released on the surface of the star, increasing momentarily the cooling rate.

During the last decades, the number of known white dwarfs increased considerably, providing extensive material to the study of this class of stars. These observations supported the comprehension of the physics that prevail inside the white dwarfs, promoting the development of very accurate stellar models. The white dwarfs stars are well-known systems, which can be used to test physics under extreme conditions that cannot be achieved in Earth laboratories.

1.3 Globular clusters

Globular clusters are old ($\gtrsim$ 8Gyrs) objects formed by a thousand to half million stars, located from near the galactic center to the foremost regions of the halo. In general, the clouds in which they were formed did not contain a large amount of metals, making them low-metallicity systems. The rotation do not play an important role on their evolution, and most of the gas and dust were expelled during their first billion year. They can be therefore generically described as old, low-metallicity, gravitationally bound stellar systems.

In figure 3 it is shown the color-magnitude diagram (CMD) of the globular cluster 47 Tucanae. The CMD is a plot in which the color and magnitude of the stars are marked. The position of the stars in the CMD depends on the evolutionary phase they are at. For instance, the stars on the right part of the diagram are mainly main-sequence stars, while the stars on the left part are white dwarf stars.

In the CMD of figure 3 all the stars are supposed to have approximately the same age and metallicity, as they all belong to the same cluster. The age and metallicity of a cluster can be derived by combining evolutionary models with the observed CMD. The most common method to derive the age of a cluster is by identifying the mass of the stars

that are leaving the main sequence, using the main-sequence turnoff point. In the CMD of 47 Tucanae the turnoff point can be observed at magnitude ~ 3.5.

Because of the considerable age of the globular clusters, it is expected that a sizable white dwarf population has been formed in these objects. The observation of these stars could tell us about the whole evolution of the cluster, as the white dwarfs carry information about previous phases. In particular, the white dwarfs can also be used to determining the age of a cluster. 47 Tucanae is one of a few globular clusters which have available data from very dim white dwarfs and for which it is possible to observe a turn to bluer colors at the end of the white dwarf sequence. The position of this blue turn combined with evolutionary models can be used to determine the age of the cluster.

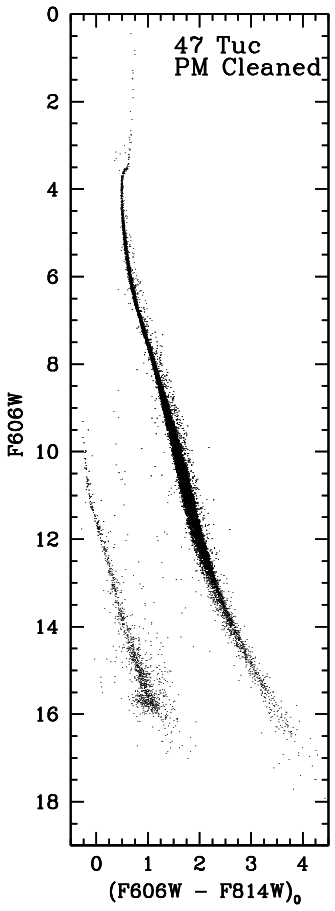

Figure 3 – Color Magnitude Diagram of the globular cluster 47 Tucanae. On the right rely the main sequence stars, and on the upper part the main sequence turn-off is evident. On the left it is shown the white dwarf cooling sequence. Image from [1]

1.4 Dark Matter

In the 17th century, with the discovery of otherwise unseen objects thanks to the telescopes, the idea that the Universe may contain matter that cannot be perceived by ordinary means gained further support [15]. During the following centuries, there were several studies searching for invisible objects, and some of them lead to the discovery of planets and stars. At the beginning of the 20th century, there were the firsts attempts to estimate the amount of dark matter in the Milky Way, but they lead to the misconclusion that the presence of large amounts of unseen matter was unlikely.

The first pieces of evidence of the existence of dark matter arose during the 1930s, with the pioneering works from Fritz Zwicky and Sinclair Smith. The most famous of them, Zwicky noticed a scatter in the velocities of some galaxies in the Coma Cluster and applied the Virial theorem in order to estimate its mass. Smith, on the other hand, assumed that the outer galaxies in the Virgo cluster were in a circular motion to estimate its total mass. Although they used different methods, both concluded that was too much mass-per-galaxy. Zwicky attributed this missing mass to "cool and cold stars, macroscopic and microscopic solid bodies, and gases" [16], while Smith assigned to "internebular material, either uniformly distributed or in the form of great clouds of low luminosity surrounding the [galaxies]" [17].

For the next 30 years, there were numerous works trying to explain the mass discrepancy, and several others questioning the findings of Zwicky and Smith. Yet, the problem was not established until the 1970s, when optical measurements of the outer parts of galaxies became available. Vera Rubin and Kent Ford published high-quality measurements of the radial velocity of M31 in 1970 [18], showing that the radial velocity remains constant even when the luminosity of the galaxy drops. Their measurements were in agreement with the radio measurements of the even outer parts of the galaxy, reported previously by Morton Roberts in 1966 [19].

In the same year, Freeman compared the radius at which the rotation curve of some galaxies was predicted to peak to the observed 21 cm (radio observations) rotation curve, and concluded that "if [the data] are correct, then there must be in these galaxies additional matter which is undetected, either optically or at 21 cm." [20]. During the following years, many scientists dedicated themselves to the problem of the dark matter, that is now well established.

1.4.1 Evidence of the existence of dark matter

1.4.1.1 Velocity dispersion

The Virial theorem can be used to measure the mass distribution in a bound and relaxed system. It can be applied to systems like elliptical galaxies and galaxy clusters.

The Virial theorem can be written as:

$$\langle K\rangle = -\frac{1}{2}\langle U\rangle,$$

where $\langle K\rangle$ is the average kinetic energy and $\langle U\rangle$ is the average potential energy. Replacing $\langle K\rangle = \frac{Nmv^2}{2}$ and $\langle U\rangle = \frac{N^2Gm^2}{2r}$, where N is the number of objects in the system, G is the gravitational constant, and v, m and r are the velocity, mass, and distance of the objects, we obtain

$$Nm = M_{total} = \frac{-2r\langle v\rangle^2}{G}.$$

It is possible to estimate the mean velocities (e. g. Doppler shift), and thus obtain the mass of the galaxies and/or galaxy clusters. This was done for the first time almost a century ago by Fritz Zwicky for the Coma cluster [16], and the conclusion was that the mass to luminosity ratio of this system had to be much larger than the ratio of mass to light for stars in the local solar neighborhood.

This discrepancy between the ratio of mass to light has been detected for many systems after that, driving to the conclusion of the needing for additional mass which does not interact with radiation [21].

1.4.1.2 Galaxy Rotation Curves

The rotation curve of a disc galaxy shows the radial velocity of objects of the galaxy as a function of their radial distance. In Newtonian dynamics, the radial velocity of an object in stable orbit at a distance r from the center of the movement is given by

$$v(r) = \sqrt{\frac{GM(r)}{r}},$$

where $M(r) = 4\pi \int \rho(r)r^2dr$.

For sufficient long distances from the center of the galaxy, the luminosity drops, and therefore, also should the density. Considering that the mass of the galaxy is enclosed in the visible radius, the velocity of any object outside it should be given by

$$v(r) = \sqrt{\frac{GM_{enclosed}}{r}}.$$

It means that the velocity of the objects outside the visible galaxy is expected to fall. However, observations of the velocities of the outermost regions show that the velocity is not decreasing, but rather is approximately constant.

To account for a constant velocity, it is necessary to assume a halo with $M(r) \propto r$ (or $\rho \propto r^{-2}$). In Figure 4 it is shown the expected rotation curve predicted by the visible

matter, and the rotation curve of the galaxy Messier 33 obtained with observations. The optical image of the galaxy is indicated for reference. It can be seen that the radial velocity does not fall even far from the edge of the visible galaxy. The same occurs with our own galaxy.

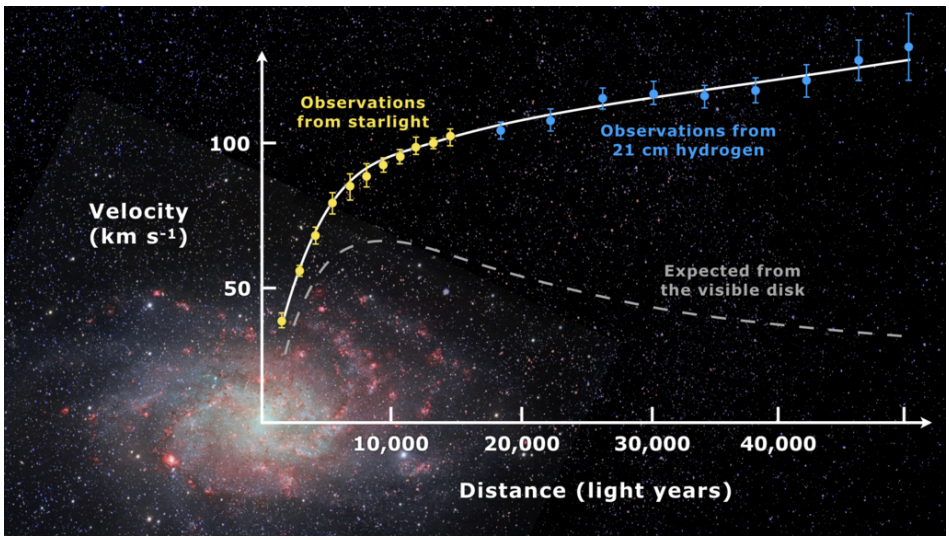

Figure 4 – Rotation curve of spiral galaxy Messier 33 (yellow and blue points with error bars), and a predicted one from distribution of the visible matter (gray line). The discrepancy between the two curves can be accounted for by adding a dark matter halo surrounding the galaxy. Image taken from Wikipedia

1.4.1.3 Cosmic Microwave Background (CMB)

The cosmic microwave background is the oldest electromagnetic radiation we can see. The photons from the CMB were emitted just after the recombination of the Universe, and are the firsts ones to be able to travel without being absorbed or deviated by ions.

Measuring the photons from the CMB allows us to analyze the temperature anisotropies in different regions and scales of the primordial universe. The angular power spectrum of the anisotropies is observed to contain a series of acoustic peaks. Those peaks can be predicted by a set of cosmological parameters, which can be matched to the data to be constrained.

The content of the primordial universe is a determining factor in the pattern of peaks-and-valleys that will arise in the CMB, and dark matter is necessary to fully reproduce the data. As dark matter does not interact directly with radiation, ordinary and dark matter perturbations evolve differently with time. The imprints of them in the CMB power spectrum are, therefore, presumably different.

In Fig 5 it is shown the power spectrum of the fluctuations from Planck data. The several peaks and valleys provide strong evidence of the existence of the dark matter, as they can be well fitted by the ΛCDM (cold dark matter) model.

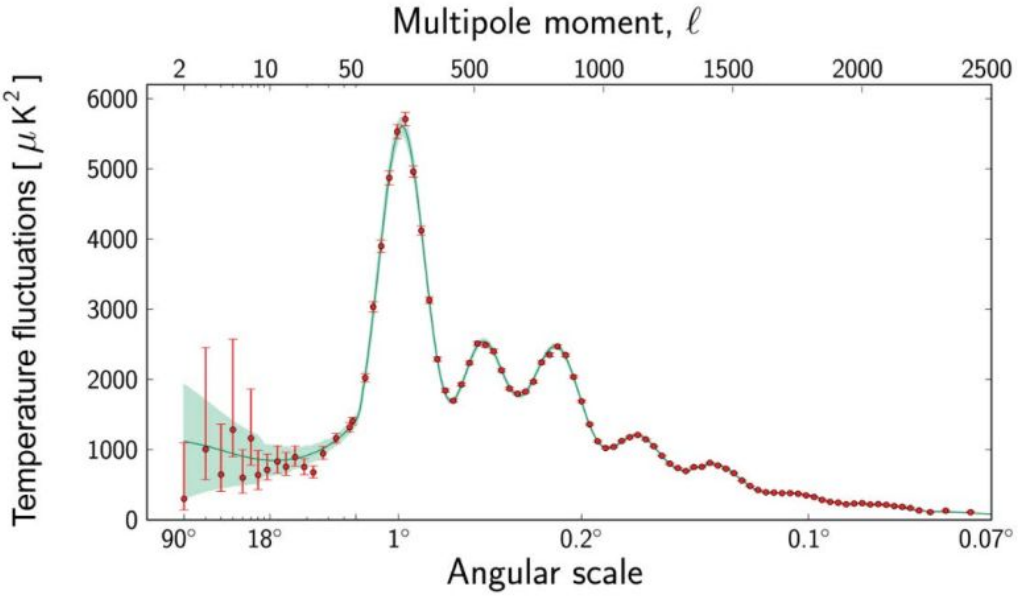

Figure 5 – Power spectrum of temperature fluctuations in the cosmic microwave background. Red dots are the Planck data, and the green curve represents the ΛCDM model. Image taken from NASA/IPAC Extragalactic Database page.

1.4.1.4 Structure Formation

Structure formation is the formation of large-scale objects such as galaxies and clusters of galaxies from the density fluctuations of the beginning of the universe. The small fluctuations of the early universe had to grow and condense to form the stars, galaxies, and larger structures. The baryonic matter is, however, affected by the radiation, which was dominant at the beginning of the universe. The small fluctuations would therefore vanish and the structures would not be formed as we see them if the matter were formed only by baryonic matter. As dark matter is not affected by the radiation, it is pointed as a solution to this problem.

1.4.1.5 Gravitational lensing

As gravity locally changes the geometry of spacetime, a sufficiently intense gravitational field deviates the light. By doing it, it is possible to actually see objects that are behind the object that causes the intense gravitational field. This phenomenon is called gravitational lensing, as the massive object acts as a lens, deflecting light. By measuring the distortion geometry, the mass of the massive object can be calculated.

The determination of the mass of the objects by using this method has giving a much higher mass to light ratio than for stars in the solar neighborhood. It leads to the to conclusion of the need of additional mass which do not emit light.

1.4.1.6 Cluster collisions

The observation of galaxy cluster collisions is an important evidence of dark matter. As the main components of the galaxy clusters (stars, gas and dark matter) behave differently during the collision, they can be studied separately. The most famous example of the use of cluster collision for dark matter evidence is the Bullet Cluster (Figure 6). The individual galaxies are all along the image, while the gas is shown in two distributions near the center. While the individual galaxies rarely interact with each other, the gas is more likely to interact. Because of this, part of the gas assumes the form of a "bullet", giving rise to the name of the cluster. The matter concentration do not follow either the galaxies (stars) and the gas. The matter has to be, therefore, something else.

Figure 6 – Composition of optical, x-rays and gravitational lensing observations of the bullet cluster. The optical image data reveals the individual galaxies, the x-ray image reveals the cloud of hot gas in red, and the blue clouds show the distribution of dark matter in the cluster, determined with gravitational lensing. Image taken from APOD page.

Many other collisions were already observed, allowing constraints of the dark matter interactions [22].

1.4.1.7 Other evidences

The ΛCDM model has also been successful in reproducing many other phenomena, like the abundance of light elements in the primordial universe (primordial nucleosynthesis), the Lyman alpha forest measurements, and the distances measures of type 1A supernovas.

1.4.2 Dark matter characterization

Although we still do not know what dark matter is made of, several properties can help us to limit the possible dark matter candidates. Taoso, M and collaborators proposed, in 2008, a 10-point test that a new particle has to pass to be considered a viable dark matter candidate [23]:

(i) Does it match the appropriate relic density?

The abundance of baryons and matter is given by:

$$\Omega_b h^2 = 0.0220^{+0.0006}_{-0.0008} \quad \Omega_M h^2 = 0.131^{+0.004}_{-0.010}$$

While the abundance of baryons is consistent with the determination from big bang nucleosynthesis, there is still a huge amount of undetected matter that is called dark matter. The abundance of any particle that aims to explain the dark matter has to correctly reproduce the value of the relic density to solve the dark matter problem. Moreover, its lifetime must exceed the present age of the Universe (4×10^{17}s).

(ii) Is it cold?

The structure formation of the universe is supposed to depend on dark matter concentrations at the time of recombination, and the property of the dark matter to form clumps before that time is the key property. This property is connected to the velocity of the dark matter particles, which can be categorized into cold, warm, and hot dark matter. The hot dark matter particles would have relativistic velocities during recombination, and as the high velocities would prevent the dark matter to form clumps, the idea of a hot dark matter is disfavored. The standard theory of structure formation requires the Dark Matter to be cold (non-relativistic particles).

(iii) Is it neutral?

As dark matter is believed to not interact with eletromagnectic radiation, any particle that can explain the dark matter content of the universe should be neutral.

(iv) Is it consistent with Big Bang nucleosynthesis (BBN)?

Big Bang Nucleosynthesis predicts the abundances of light elements produced soon after the Big Bang, and the observations agree pretty well with the theory. Any particle proposed to be dark matter cannot change the initial abundances of the elements.

(v) Does it leave stellar evolution unchanged?

"Stellar evolution provides a powerful tool to constrain particle physics, providing bounds that are often complementary to those arising from accelerator, direct and indirect Dark Matter searches." [23]

Dark matter candidates could be produced inside the stars and, depending on their interactions, be able to alter the stellar evolution. However, the evolution of stars is bounded by high-quality observations, and any particle proposed must not alter significantly the properties of the stars.

(vi) Is it compatible with constraints on self-interactions?

Observations of the galaxy centers, halos, and galaxy cluster collisions constrain the possible cross-section of self-interactive particles.

(vii) Is it consistent with direct dark matter searches?

Many dark matter experiments have been built during the last years. Most of them aim to detect dark matter particles through the nuclear recoil produced by scattering. With those experiments, it is possible to either confirm or exclude some parameters of the dark matter particles.

(viii) Is it compatible with gamma-ray constraints? and (ix) Is it compatible with other astrophysical bounds?

The search for dark matter particles is not limited to direct detection. The dark matter candidates can generate sub-products in their interactions, such as photons, anti-matter, and neutrinos. The non-observance or observance of excess of those particles can constrain the dark matter characteristics. The astrophysical observations are, thus, an important tool to prove the dark matter candidates.

(ix) Is it compatible with other astrophysical bounds?

There can be other astrophysical bounds apart from stellar evolution that can invalidate a dark matter candidate. The specific evidence depends on the candidate.

(x) Can it be probed experimentally?

We have to be able to detect or at least collect strong evidence of the existence of one dark matter candidate, otherwise we would never know if the particle does exist.

1.4.3 Dark matter candidates

1.4.3.1 MACHOs

MACHOS (Massive Compact Objects) are massive objects that do not emit or emit very little eletromagnetic radiation. These objects can be planets, cold stars, or black holes. Although they do not emit light, they could be detected by gravitational microlensing.

One promising candidate of this class is the primordial black holes, that should be formed soon after the Big Bang. However the existence of MACHOS has been tested for several years, and it is now excluded that they could contribute significantly to the dark matter over most of the plausible mass range [24].

1.4.3.2 Sterile Neutrinos

By the theory of the Standard Model, neutrinos should be massless. However, observational evidence of the oscillation of neutrinos leads to the conclusion that they should have mass. The existence of neutrino masses inferred by observations could be explained by a right-handed neutrino, the so-called sterile neutrino.

The sterile neutrinos are expected to interact only by gravity, and, if they are heavy enough, could explain cold or warm dark matter.

1.4.3.3 WIMPs

The WIMPs (Weak Interactive Massive Particles) are hypothetical massive particles that are found in many-particle physics theories and can explain dark matter. Two examples are the Neutralinos, which are predicted to exist by the supersymmetry (SUSY) model, and the Kaluza-Klein particle (KKP), which arises from the universal extra dimension theory (UED).

1.5 Axions

The axion is a pseudoscalar boson [25, 26] that emerges from a solution of the Strong CP problem, proposed by Peccei and Quinn [27]. It is a necessary consequence to explain the non-violation of the CP symmetry in strong interactions. Besides its relevance to the Standard Model, the axion is pointed out as a candidate for cold dark matter [28, 29].

1.5.1 Strong CP problem

The Standard Model of particle physics has been shown to be successful in describing visible matter, explaining practically all data in terms of a small number of parameters. Despite the success in describing most of the particle interactions, there are some unsolved issues in the model. One of the most puzzling questions is why the strong interactions conserve CP symmetry, while there seems to be no particular reason for it to happen.

The CP symmetry refers to the combination of the charge (C) and parity (P) symmetries. The charge conjugation is a transformation that switches the particles for their antiparticles, and the parity conjugation inverts their spatial coordinates. This symmetry was observed to be violated in weak interactions and would be expected to be also violated in strong interactions. Until now, however, no violation has been observed in strong interactions. The experimental measures of the neutron dipole momentum, which would be expected to exist if the CP symmetry were violated, put a tight limit on the possible amount of CP violation (θ_{QCD}).

In 1977, Peccei and Queen proposed a solution for the strong CP problem [27], by postulating a new symmetry (PQ symmetry) that is spontaneously broken at large energy scales. A consequence of this mechanism is a new particle, the axion [26].

1.5.2 Axions as dark matter

It was soon realized that the axions could be accounted for the dark matter of the Universe [30, 31, 28, 32]. The PQ symmetry is thought to be broken during the earliest moments of the Big Bang, producing the axions [33]. The axion dynamics and the resulting dark matter density depend on when the symmetry breaking takes place, whether before or after the inflation. Regardless of when the PQ symmetry is broken, axions can be produced non thermally by the vacuum realignment mechanism [34]. The axion field begins to oscillate in its potential, and as axions are low interacting particles, the oscillations do not vanish through time [35, 36]. These oscillations, therefore, can contribute to the local density as cold dark matter.

1.5.3 Axion mass

The QCD axion has a single free parameter, the decay constant f_a, which is proportional to the energy at which the PQ symmetry is spontaneously broken. The axion mass can be written as a function of this single parameter [37]:

$$m_a = 5.691(51) \left(\frac{10^9 GeV}{f_a} \right) \quad meV. \tag{1.6}$$

In the original axion model, f_a is of the order of the electroweak scale, implying an axion that is relatively strongly coupled to the matter [36]. The original axion was soon ruled out by laboratory experiments and astrophysical considerations. Back then, stellar evolution played an important role in rejecting this heavy axion model [33].

The rejection of the heavy axion model led to the development of the "invisible" axions models, in which f_a can be arbitrarily large, and consequently m_a arbitrarily small.

1.5.4 Axion models

The most widely discussed invisible axion models are the KSVZ (Kim-Shifman-Vainshtein-Zakharov) [38, 39] and the DFSZ (Dine-Fischler-Srednicki-Zhitnitsky) [40, 41]. From a practical perspective, the difference between these two models relies on their couplings to the matter. In the KSVZ model the coupling is limited to nucleons and photons. In DFSZ axion models the axions also couple to charged leptons, like electrons.

1.5.5 Coupling to the matter

For QCD axions there is a definite relationship between mass and interaction strength. It means that the axion mass can be linked to a photon, a fermion, and/or another particles coupling constant.

For the axion coupling to photons, the relation is given by [42],

$$g_{a\gamma\gamma} = \left(0.203(3)\frac{E}{N} - 0.39(1)\right)\frac{m_a}{GeV^2}, \tag{1.7}$$

in which $\frac{E}{N}$ is the is the ratio of the Electromagnetic and the color anomaly. It is model dependent, assuming the value $\frac{E}{N} = \frac{8}{3}$ in the DFSZ model and $\frac{E}{N} = 0$ in the KSVZ model.

For the axion-electron coupling in the DFSZ model,

$$g_{ae} = \frac{C_e m_e}{f_a} = C_e 0.85 \times 10^{-10} m_a(eV), \tag{1.8}$$

where C_e is an effective PQ charge [43] and it is assumed to be 1/3 in this work.

1.5.6 Axion constraints

As the m_a is not fixed by the theory, the experiments devoted to the detection of axion consider wide ranges of masses and couplings to the matter. Several experiments, like ABRACADABRA, ADMX, MADMAX, and CAST ([44, 45, 46, 47]) has been designed to search for the axion. In figure 1.5.6 it is shown the regions in the parameter space of axion mass and axion coupling to photons that were already searched by experiments. Until now no axion had been detected, but there are still unexplored regions in this parameter space.

Complementary to these experiments, stars have been used as laboratories to constraint the coupling of axions to matter. These particles, if they exist, can be produced inside the stars thanks to the hot and dense plasma, and freely escape from them, carrying energy out of the star. This phenomenon provides some of the most powerful limits on the properties of low interacting particles, like axions [48].

The coupling of axions to the matter can be constrained by requiring that the energy loss and stellar lifetimes cannot be in conflict with the observations [49, 50]. This requirement has been applied for stars in different evolutionary stages, leading to similar constraints. The helioseismology requires a coupling constant to photons $g_{a\gamma\gamma} \lesssim 4.1 \times 10^{-10}$ GeV^{-1} [51] , the solar neutrino flux requires $g_{a\gamma\gamma} \lesssim 7 \times 10^{-10}$ GeV^{-1} [52] and the helium-burning lifetime of globular cluster stars requires $g_{a\gamma\gamma} \lesssim 6.6 \times 10^{-11}$ GeV^{-1} [53].

Considering the models where the axions couple to electrons, the most restrictive limits arises from white dwarf stars [54]. Due to the conditions inside the white dwarfs, the production of axions occurs mainly by the coupling to electrons. The first attempt to

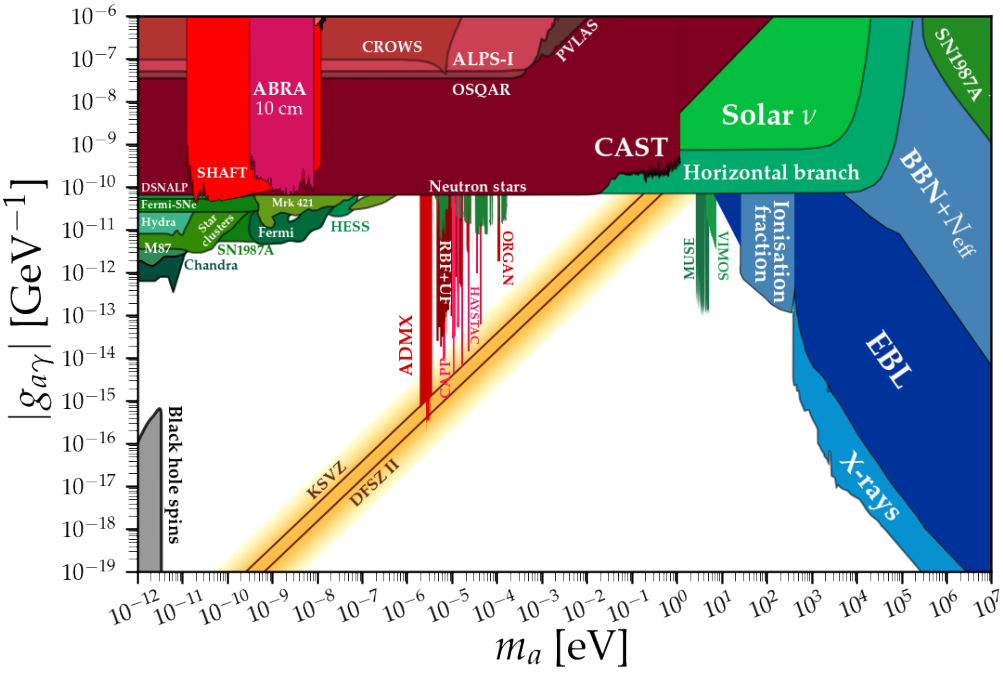

Figure 7 – Parameter space of axion mass and axion coupling to photons. Colored regions are the regions already searched by experiments or excluded by some astrophysical phenomena. The KSVZ and DFSZ models are marked in the yellow region. Image provided by Ciaran O'HARE

use the white dwarfs to constrain the axion-electron coupling was made by Raffelt in 1986 [55] using the white dwarf luminosity function. Since then, the observed data available has been expanded and improved, and more refined studies became possible [56]. The progress in stellar models also made possible the introduction of a new tool to constrain the axion-electron coupling: the pulsating white dwarfs. Exploiting the connection of the variation of pulsation period with the white dwarf cooling rate, [57] used the variable G117-B15A to constrain the axion-electron coupling. Many other studies using pulsating white dwarfs had been done since then. Up to date constraints from variable white dwarfs are: PG1351+489 $g_{ae} < 3.2 \times 10^{-13}$ [58], L19-2 $g_{ae} < 7 \times 10^{-13}$ [59], R548 $3.2 \times 10^{-13} < g_{ae} < 6 \times 10^{-13}$ [60], G117-B15A $4.7 \times 10^{-13} < g_{ae} < 6.23 \times 10^{-13}$ [61]. The values of the axion coupling to electrons can be translated to the mass of the axion by assuming the DFSZ model (equation 1.8).

2 Aims and scope

In this work I intend to explore the white dwarf cooling, searching for measurable effects that axions could cause in the cooling evolution.

The axions are yet non-observed well motivated particles, whose existence has been tested in Earth laboratories, as well as in astrophysical systems. Inside white dwarf stars, these particles would be copiously produced, carrying energy away with them. The white dwarf stars are well studied objects whose evolution is well described by evolutionary models. There are incredibly accurate observations of these objects, and any additional physical phenomenon inside them are bound by these observations.

My aim in this work is to study in detail the axion production and emission inside the white dwarfs. I plan to analyse the white dwarf evolution and identify the effects of axions. Additionally, I intend to investigate the axion emission in low-metallicity white dwarf models. I expect to be able to comprehend how the evolution of white dwarf of different metallicity could be affected by axions.

In addition, my purpose is to provide self-consistent calculations of the white dwarf cooling with different metallicities including axions with distinct couplings to electrons. These calculations can be applied to a variety of works in the future.

Even though white dwarfs have been largely used to constrain the axion-electron coupling strength, the white dwarf cooling sequence of globular clusters is still an unexplored scope in this context. The globular clusters are considered excellent laboratories for the study of stellar evolution, as they are assumed to have a simple stellar population, with same age and metallicity [62]. If the axions play an important role in the cooling times of white dwarf stars, some properties of the white dwarf cooling sequences of globular clusters can be affected by them. In this work I also intend to explore the usage of globular clusters in the attempt to constrain the axion-electron coupling.

Briefly speaking, my aims in this work are:

- Identify and understand the consequences of axion emission in white dwarf stars with different metal content, focusing on their lifetimes;
- Make use of the identified changes caused by axions to constrain the axion-electron coupling.

3 Methodology

To achieve the aims pointed in the chapter 2, I calculate self-consistent white dwarf sequences using LPCODE code (see section 3.1.1). My calculations embrace white dwarf masses from $0.524M_{\odot}$ up to $0.917M_{\odot}$ and three different initial metallicities ($Z = 0.01$, 0.004 and 0.0001). The emission of axions was implemented self-consistently for axion masses varying from 1 to 30meV ($g_{ae} = 2.8 \times 10^{-14}$ to $g_{ae} = 8.5 \times 10^{13}$). The specific values for the white dwarf masses (M_{WD}), metallicity of the progenitor (Z), and axion masses (m_a) used in this work are shown in table 1. Sequences marked with an asterisk experience a hydrogen sub-flash (see chapter 4).

M_{ZAMS}	Z=0.01		Z=0.004		Z=0.0001	
	M_{WD}	m_a	M_{WD}	m_a	M_{WD}	m_a
0.80					0.534	17*, 30*
0.90					0.550	17, 30*
0.95			0.524	17*, 30*		
1.00	0.525	17*, 30*	0.537	17*, 30*	0.569	17, 30*
1.10			0.547	17*, 30*		
1.20			0.553	17*, 30*		
1.25					0.621	17,30
1.50	0.570	1-30	0.599	17, 30	0.669	17, 30
1.75	0.593	1-30			0.708	17, 30
2.00			0.665	17, 30	0.737	17, 30
2.25	0.632	1-30	0.691	17, 30		
2.50			0.730	17, 30	0.826	17, 30
3.00	0.705	17, 30	0.817	17, 30	0.875	17, 30
3.50	0.770	1-30				
4.00	0.837	17,30				
5.00	0.877	1-24, 30				
6.20	0.917	17,30				

Table 1 – The mass, metallicity, and axion mass used in the models calculated in this work. The values for the zero-age main sequence mass (M_{ZAMS}) were extracted from [4, 3]. When a range is provided, the step is 1 meV. Sequences marked with an asterisk experience a hydrogen sub-flash.

The white dwarf sequences provided the essential material to proceed with the analysis of the axion emission in white dwarfs. The models allow us to look at features of the white dwarf models throughout the cooling, making it possible to compare models with and without the emission of axions.

The inclusion of new metallicities apart from solar metallicity in my analysis go beyond previous studies on the field and unlock new possibilities. First I compared the models with distinct metallicities to find if the axion emission show a dependence with Z.

Then I employ the low metallicity sequences to compare my theoretical calculations with real data from globular clusters to find out if there was an distinguishable age difference between the age determined with and without considering axions in the models.

To compare models with data it is necessary to convert the properties of the models such as luminosity and temperature into observable properties, such as color and magnitude. To obtain the magnitude in the HST filters F606W and F814W I use the white dwarf atmospheric tables from Pierre Bergeron[1].

To compare the computed sequences with data from a globular cluster I build white dwarf isochrones. Isochrones are the representation of same age stars that draw a line in the HR diagram. To build them, I interpolate the white dwarf models to obtain characteristics such as luminosity and effective temperature (or color and magnitude) of each sequence at a determined age.

The globular cluster I selected for this work is 47 Tucanae. For this object, the white dwarf cooling curve is observed completely, enabling us to identify the end of the white dwarf cooling sequence. Furthermore, 47 Tucanae is the globular cluster with more detected white dwarfs. It is relevant to highlight that 47 Tucanae was already studied using the same evolutionary code I used (LPCODE), giving us a consistent way to compare the effect of the axions in the age determination.

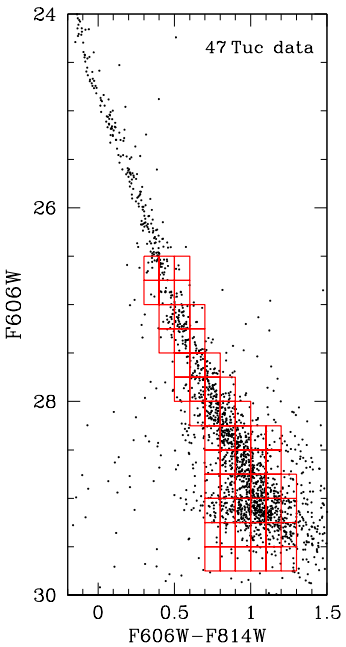

Figure 8 – The red grid overlaid on the white dwarf cooling sequences of 47 Tuc illustrating the way the data were binned in order to compare the observations to the Monte Carlo simulations with Hess diagrams. Figure taken from Campos et al. (2016) [2].

[1]The atmospheric tables are available in the Pierre Bergeron website

I used a population synthesis code to generate artificial CMD from the isochrones, which simulates the stars as seen in observations (see section 3.1.2). To reduce model uncertainties I generated the simulations with 20 000 stars and after I normalized it to have the same number stars as 47 Tucanae. To compare the simulations with observations I used Hess diagrams binned with a grid width of 0.1 mag in F606W-F814W and 0.25 mag in F606W, a grid identical to that used in previous analysis of the same data [2], as shown in Figure 3. Then I searched for the theoretical CMD that better matches the observations using a χ^2 minimization:

$$\chi^2 = \sum_i \frac{(O_i - E_i)^2}{\sigma_{O_i}^2}, \tag{3.1}$$

where E_i is the number of events expected according to the model, O_i is the number observed in the ith bin and, as we assume our data follow a Poisson distribution, σ_{O_i} is the uncertainty in the number of observed stars ($\sqrt{O_i}$). After these values were normalized to the minimum value.

3.1 Numerical Methods

I use some numerical tools to perform the necessary calculations in this work. The stellar evolution models were calculated employing LPCODE evolutionary code, described in Section 3.1.1; and the white dwarf cooling sequence simulations were calculated by making use of a Monte Carlo simulation, described in Section 3.1.2.

3.1.1 LPCODE

The evolutionary computations presented in this work were calculated with the LPCODE evolutionary code, described in detail in [63, 6, 4, 64]. LPCODE computes the complete evolution of a single star from the zero-age main sequence (ZAMS), through the hydrogen and helium burning stages, through the thermally pulsating, and mass-loss stages on the AGB, to the white dwarf cooling evolution. This code has been employed to produce very accurate white dwarf models (see [6, 65, 4] and references therein), and to study the emission of axions ([59] [66] [60] [13]).

In LPCODE, spherical symmetry is adopted, meaning that effects of rotation and magnetic field are not included. Also, hydrostatic and thermal equilibrium are assumed. The basic equations to be solved are:

$$\text{Conservation of mass:} \quad \frac{\partial r}{\partial m} = \frac{1}{4\pi r^2 \rho}, \tag{3.2}$$

$$\text{Hydrostatic equilibrium:} \quad \frac{\partial P}{\partial m} = -\frac{Gm}{4\pi r^4}, \tag{3.3}$$

$$\text{Energy conservation:} \quad \frac{\partial l}{\partial m} = \epsilon_{nuc} - \epsilon_{\nu} - c_p \frac{dT}{dt} + \frac{\delta}{\rho}\frac{dP}{dt}, \tag{3.4}$$

$$\text{Energy transport:} \quad \frac{\partial T}{\partial m} = -\frac{GmT}{4\pi r^4 P}\nabla, \tag{3.5}$$

where r is the radial distance to the center of the star, m is the mass, ρ is the density, P is the pressure, l is the luminosity, t is the time, ϵ_{nuc} is the nuclear energy emission rate, ϵ_{ν} is the neutrino emission rate, T is the temperature, c_p is the specific heat, $\delta = \frac{\partial ln\rho}{\partial lnT}$, and ∇ is the temperature gradient.

These equations cannot be solved analytically, and numerical calculations are required. To perform the calculations, the equations are linearized and treated discretely. The equations are solved iteratively, by a Newton-Raphson like method, known as the Henyey method.

The chemical composition of a star model is modified by nuclear reactions and mixture. It is given by a set of coupled partial equations which describe the temporal evolution of the chemical species in the model. The chemical composition is not calculated at the same time as the equations of structure, but alternating with the structure equations. Small temporal steps are therefore required. In LPCODE, both the step between layers and the temporal steps are adaptive, becoming small when the modeled star passes through rapid changes.

Assuming the effects of axions are negligible before the white dwarf phase, I do not calculate models since the beginning of the star evolution. I consider white dwarf initial models at the beginning of the white dwarf cooling sequence. The initial models were taken from the work of Romero (2015) [3]. For a detailed description about the pre-white dwarf calculations see [3].

3.1.1.1 White dwarf cooling models

The white dwarf cooling process calculations of this work use the same physics as in Romero (2015)[3], except for the inclusion of axion emission.

For the white dwarf phase, the equation of state of Magni and Mazzitelli (1979) [67] is used. Although white dwarfs do not have nuclear reactions in their cores, there are still residual nuclear burning in the upper layers, mainly at high luminosity. In LPCODE the nuclear reactions are taken in account until $log(L/L_{\odot}) = -4$. The important nuclear reaction rates in the white dwarf phase were taken from Caughlan and Fowler (1988) [68].

Throughout the evolution, several processes change the distribution of chemical abundances in the star. The chemical rehomogenization of the inner carbon-oxygen profile is induced by Rayleigh-Taylor instabilities, and it is included in LPCODE following Salaris (1997) [69]. The processes of gravitational settling and chemical diffusion were also taken into account, while radiative levitation is disregarded as it is only important at high effective temperatures. The chemical diffusion is based on Burgers 1969 [70], and considers the diffusion of ^{1}H, ^{3}He, ^{4}He, ^{12}C, ^{13}C, ^{14}N, ^{16}O [71]. Because of the effects of the diffusion and gravitational settling, the most heavy elements go to the innermost layers of the star, while the lighter elements stay on the upper layers.

To account for the adaptable mass fraction of the envelope, which is computed consistently accordingly to the element diffusion, I considered radiative opacity tables from OPAL [72]. For low effective temperatures (below 10 000K), I included the effects of molecular opacity [73]. The convection was treated in the formalism of the mixing-length theory, in its ML 2 parametrization, with $\alpha = 1$ [74].

The star releases energy not only by photon but also by neutrino emission. Neutrinos are produced inside them by several processes which are considered in the LPCODE. The neutrino emission rates for pair, photo, and bremsstrahlung processes were those of [12], while for plasma processes the treatment presented in [75] is included.

At low temperatures ($\sim 5\,000$K) the white dwarf core starts to crystallize. During the crystallization, the species in the core reorganize themselves in a process called phase separation. The crystallization process takes place when the ion coupling constant Γ (equation 1.5) is greater than 220 ([76]). This process releases gravitational energy, which has important consequences on the white dwarf cooling times.

The energy stored in the white dwarfs can also be carried away by some hypothetical low interacting particles. In the next section, it is described the implementation of axion emission in LPCODE, which is considered for this work.

3.1.1.2 Axions subroutines

Inside the white dwarfs, axions can be produced by three main processes: pair annihilation, Compton scattering, and bremsstrahlung. The pair annihilation process is strongly suppressed by the degeneracy and thus is not considered in my calculations.

For the Compton scattering process,

$$\gamma + e^{-} \rightarrow e^{-} + a,$$

the energy-loss rate per unit mass is calculated according to Raffelt (1995) [77]:

$$\epsilon = 33 \times \alpha_{a26} \times Y_e T_8^6 F \quad ergs \cdot g^{-1} \cdot s^{-1}, \tag{3.6}$$

in which $\alpha_{a26} = \frac{g_{ae}^2}{4\pi 10^{-26}}$ is the axion fine constant, Y_e is the electron number fraction per baryon and T_8 is $\frac{T}{10^8}$.

The bremsstrahlung process,

$$e^- + Z \rightarrow e^- + Z + a,$$

was included in the LPCODE considering three regimes. The non degenerate bremsstralung emission rate was taken in account based on Raffelt 1996 [43]:

$$\epsilon = \frac{128}{45\sqrt{\pi}} \left(\frac{\alpha^2 \alpha_a}{m_e}\right) \left(\frac{T}{m_e}\right)^{\frac{5}{2}} \frac{n_e}{\rho} \times S \quad ergs \cdot g^{-1} \cdot s^{-1}, \tag{3.7}$$

in which $\alpha = \frac{1}{137}$ is the fine structure constant, $\alpha_a = \frac{g_{ae}^2}{4\pi}$ is the axion fine constant, m_e is is the electron mass, n_e is the electron number density, ρ is the density and S is a sum that takes into account the screening effects.

The axion production in the degenerate plasma is dependent on the correlation between ions (Γ) (equation 1.5). In the case in which the ions are weakly correlated ($\Gamma < 1$), the emission via bremsstrahlung was considered following [77]:

$$\epsilon = \alpha_{a26} \times 10.8 \frac{Z^2}{A} T_8^4 F \quad ergs \cdot g^{-1} \cdot s^{-1}. \tag{3.8}$$

The degenerate case in which the ions are strongly correlated (Γ>1) was included based on the calculations of [78]

$$\epsilon = 1.08 \times 10^{23} \alpha_a \frac{Z^2}{A} T_7^4 F \quad ergs \cdot g^{-1} \cdot s^{-1}. \tag{3.9}$$

As most of the material of a white dwarf is in a degenerated state and the Γ for white dwarfs is typically larger than 1, the bremsstrahlung in degenerate plasmas with $\Gamma > 1$ (equation 3.9) is the dominant process of axion production inside the white dwarfs.

3.1.2 Population synthesis code

By performing theoretical calculations of the white dwarf cooling, we are able to determine characteristics such as effective temperature, luminosity and radius for an individual stellar mass at a given age. The evolution of a single star, however, does not take into account the probability of a star of this specified mass to form or to be detected by a telescope.

The capability to observe a star of a specified mass in a cluster is strongly dependent on the probability of this star to form, on its luminosity, on the resolution of the telescope, if it is near to other star or behind a cloud, and many other factors. In general, the

observations have large uncertainties, and the detected stars appear scattered in the color magnitude diagram. To be able to compare the theoretical calculations and the observed data set, it is important to consider these factors. In this work I used a population synthesis code, including the effects of

- the initial mass function, which gives the probability of a star of a particular mass to be formed;
- the initial to final mass relation, with which we can calculate the white dwarf mass of a star, given its initial mass;
- and the uncertainties in the observations, which are translated in the probability to a star to be observed and the scatter in the color-magnitude diagram.

I used my isochrone models produced with LPCODE to generate Monte Carlo simulations of the white dwarf populations and compared them with the observed white dwarf cooling sequences.

The code generates synthetic main-sequence stars considering a single burst star formation and a Salpeter [11] distribution for the present-day local mass function ($dN/dM \propto M^{-\alpha}$). The α was set accordingly to the α determined by Campos (2016) [2].

The initial to final mass relation (IFMR) considered is the one obtained with the full sequences of metallicity $Z = 0.004$ models used in this paper, presented in Romero (2015) [3]. I emphasize that the models - and consequently the IFMR - take in account the metallicity of the progenitors.

In this program I did not take into account the effect of multiple star formation bursts, unresolved binaries or multiple populations.

Once I had the white dwarf mass distribution of the simulated stars, I was able to generate a simulation of determined age containing the desired number of stars. In order to estimate the ages that best fit the observed data I computed χ^2 tests, as explained in Campos (2016) [2].

As my aim is not to obtain the best parameters for the cluster but rather estimate the effect of axions on the age of the clusters, I choose to use the values obtained by Campos (2016) [2] for reddening, distance modulus and α.

4 Results

The self-consistent calculations of the white dwarf evolution allow us to analyze how the cooling of the white dwarf can be affected by the emission of axions.

4.1 White dwarf models

4.1.1 The axion emission

In this work I considered the emission of axions produced by the bremsstrahlung and Compton process. The axion emission rate was self-consistently included in the white dwarf models using equations 3.6, 3.7, 3.8 and 3.9. The axion emission during the white dwarf cooling for a particular axion coupling and a particular white dwarf model is shown in Figure 9. For this plot I used a representative model of $0.632 M_{\odot}$, $Z = 0.01$ with $g_{ae} = 4.8 \times 10^{-13}$ ($m_a = 17$ meV). The emission via Compton and bremsstrahlung process consistently falls during the white dwarf cooling, varying from $\sim 100\times$ the solar luminosity at the beginning of the white dwarf phase, to values lower than $10^{-8} L_{\odot}$ for $T_{\rm eff} < 3\,500$ K. Both the emission rates present a "knee" at $\sim 4\,000$ K due to the white dwarf phase transition (see details in section 4.1.2). The emission via the bremsstrahlung process is higher values than via Compton process throughout the cooling of the white dwarf, growing

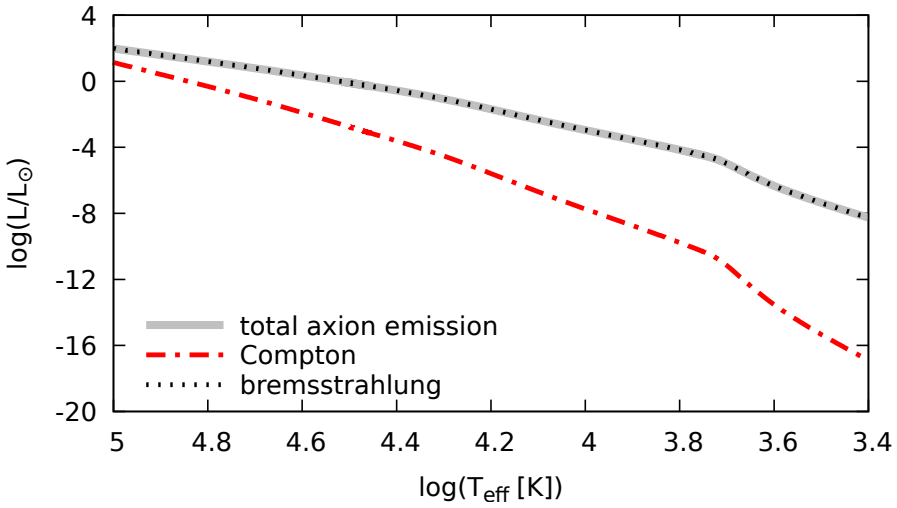

Figure 9 – Comparison between the emission of axions due to the Compton scattering and bremsstrahlung in a $0.632 M_{\odot}$ white dwarf model, considering 17 meV axions ($g_{ae} = 4.8 \times 10^{-13}$). The black dashed line shows the emission of axions via bremsstrahlung, the red dashed/dotted line shows the axion emission via Compton, and the filled gray line shows the total axion emission.

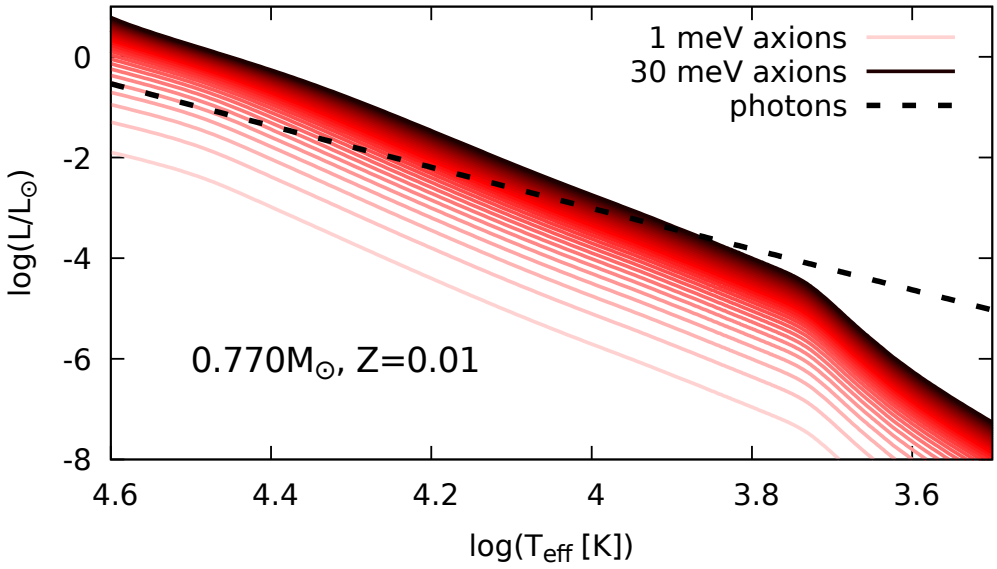

Figure 10 – The luminosity due to axions of 1 to 30 meV in a $0.770 M_{\odot}$ model. The light red line is for 1meV axions, and darker colors represent heavier axions. The dotted black line shows the luminosity due to photons.

the disparity as the star cools down. Not much is lost, therefore, if one chooses to consider only the bremsstrahlung process during the white dwarf cooling.

In figure 10 I show the luminosity due to axion emission on a $0.770 M_{\odot}$ white dwarf for axions from 1 to 30 meV. I plot the photon luminosity for reference. The contribution of the axion emission to the white dwarf cooling will depend on the axion mass. The luminosity of the 1 meV axion is at least 100× lower than the photon luminosity, thus representing a minor source of energy loss. The luminosity of the 30 meV axion can be at least 10× higher than the photon luminosity.

4.1.2 Axion effects on the inner structure

To study the impact of axion emission on the inner structure of white dwarfs I consider a representative model characterized by $M = 0.632 M_{\odot}$ and $T_{\rm eff} = 25\,700$ K. In the upper panel of the Figure 11 I show the axion luminosity as a function of the mass ($m(r)$) for an axion coupling of $g_{ae} = 4.8 \times 10^{-13}$ ($m_a = 17$ meV). In the bottom panel I show the chemical and density profiles for reference. The axion emission, which was already shown to be dominated by the bremsstrahlung process (equation 3.9), is approximately constant in the core of the white dwarf, and drops considerably in the outer parts. The emission can therefore be described as having a constant value and occurring only in the core of the white dwarf. The almost-constant emission in the core is caused by the almost-constant core temperature, on which the emission rate depends as T^4. The chemical transitions are also responsible for the changes in the axion emission in the white dwarf, although the

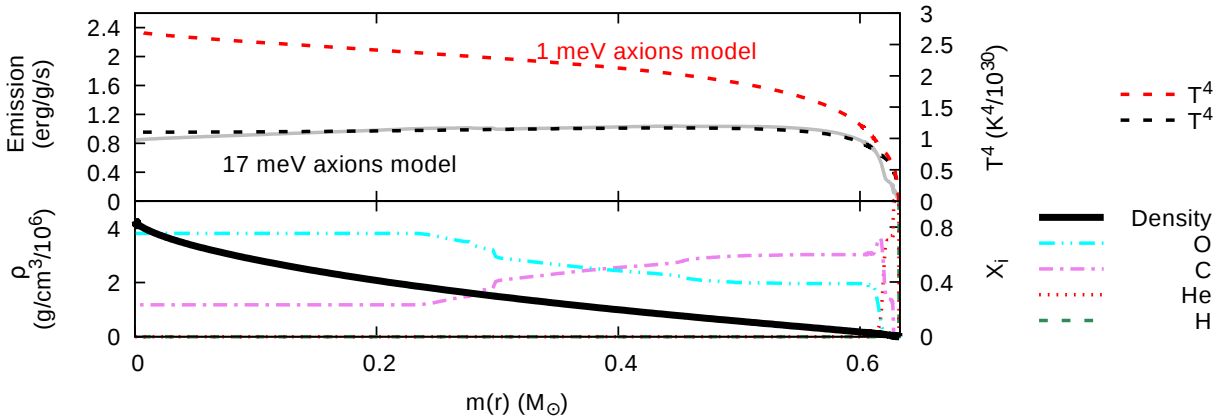

Figure 11 – Profile of a $0.632M_{\odot}$, $Z = 0.01$ white dwarf model at $T_{\rm eff} \approx 25\,700$K. In the bottom panel, it is shown the density (ρ) (black continuous line) and the abundances (X_i) of H, He, C, and O. In the top panel it is shown the temperature to the fourth power for the model including 1 meV axions (red dashed line) and including 30 meV axion (black dashed line), and the axion emission (gray continuous line).

sudden slope above the core should be also addressed to the degeneracy transition.

In addition to the axion emission rate, I show in figure 11 the T^4 profile of the 17 meV model, as well as the T^4 profile of a model of same mass, metallicity and effective temperature but considering 1 meV axions. Despite the models having the same effective temperature, the temperatures in the core are not identical. The temperature of the 1 meV model systematically increases towards the center, while the temperature of the model including higher axion mass is roughly constant in the core. It indicates that the axions are capable of altering the thermal structure of the white dwarf. Axion emission removes energy from the star, and as higher the temperature the higher is the emission rate. The implications of it will be discussed in subsection 4.1.3.

In figure 12 I show the central temperature during the white dwarf cooling for models of 0.665 and $0.817M_{\odot}$ and $Z = 0.004$. I present the axion-less model, as well as the models calculated including 30meV axions. The effect of axion emission on the central temperature starts to be measurable at the beginning of the cooling sequence, at around $T_{\rm eff} \sim 100\,000$K. The maximum difference in T_c is around $T_{\rm eff} = 30\,000$ for both masses. I estimated the reduction of the central temperature due to axions as reaching $\sim 30\%$, independent of the white dwarf mass. Despite that, after some time the central temperature is not affected anymore by the presence of axions. Below $T_{\rm eff} \approx 10\,000$K the central temperature of the models with and without axions are basically the same. I conclude that axions can have a significant impact on the central temperature of white dwarfs hotter than $\sim 20\,000$K, while the colder ones are essentially unaffected.

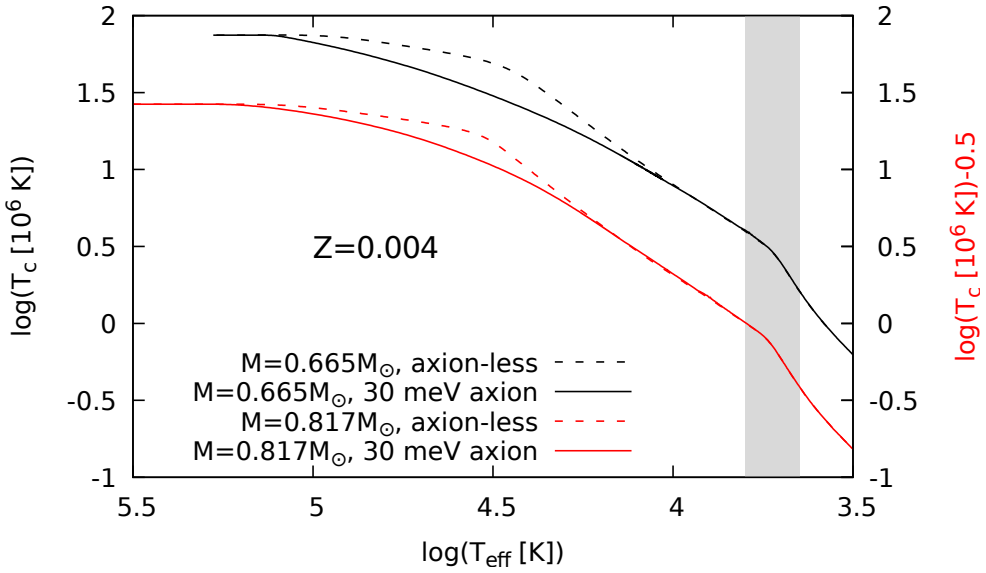

Figure 12 – Central temperature in function of the effective temperature for models with M=0.665$M_\odot$ (black lines) and M=0.817$M_\odot$ (red lines), with 30 meV axions (continuous line) and axion-less (dashed lines). The gray area marks the occurrence of convective coupling.

4.1.3 Implications of axion emission

The change in the thermal structure caused by axions has implications on the processes dependent on the temperature. In Figure 13 it is shown the emission of photons, axions, and neutrinos for models with $M_{WD} = 0.632M_\odot$, $Z = 0.01$, including and not including $m_a = 17$ meV axions ($g_{ae} = 4.8 \times 10^{-13}$). The emission of neutrinos is strongly dependent on the temperature ($\epsilon \propto T^7$), and can be seen to be lower in the model in which axions were included, when compared to the axion-less model. A detailed discussion about the axion impact on the neutrino emission can be found on [13]. Here I limit myself to stress that the axion emission must be implemented non perturbatively to be consistent with the other sources of energy loss, specially for axion masses above 10 meV and effective temperatures higher than 20 000K.

Not only the emission of neutrinos but also the emission of axions itself is affected by the reduction of the core temperature. The overestimation of the axion emission by a perturbative approach can be of order 2× the emission calculated in self consistent models at $T_{\rm eff} \sim 30\,000K$.

Despite the effect of axions on the core temperature of white dwarfs, the evolution of a white dwarf in the HR diagram is left mostly unaffected. The relation between the luminosity and effective temperature is not modified, making it in general impossible to distinguish a sequence with axions from an axion-less sequence by its HR diagram. Only a few sequences with axions can be distinguished from the axion-less counterpart, and these

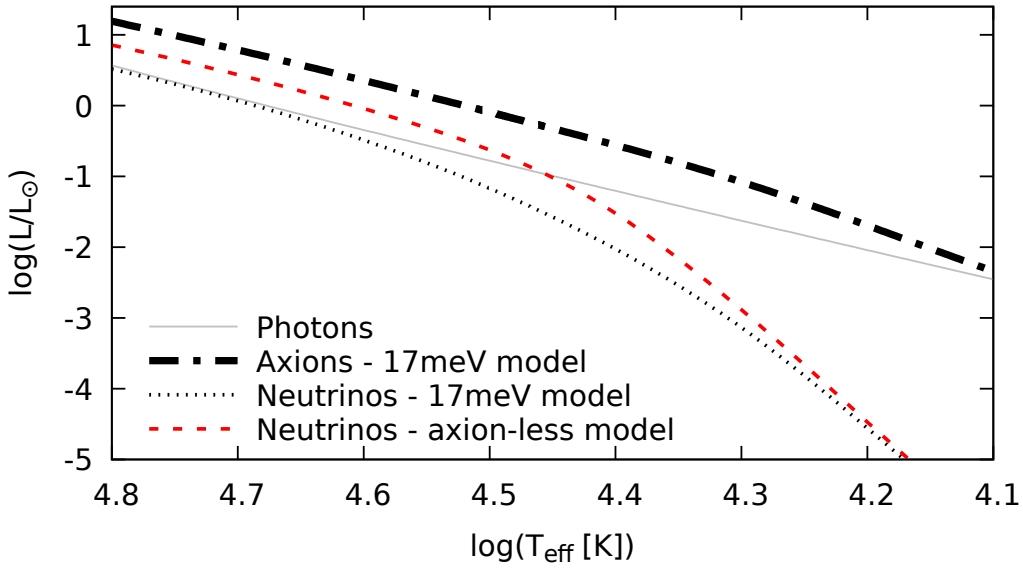

Figure 13 – Luminosity of the emission of photons (gray continuous line), neutrinos (dashed and dotted lines), and axions (dashed-dotted line) as a function of the effective temperature for models of $0.632M_{\odot}, Z = 0.01$. The neutrino emission is given for the axion-less models (red dashed line) and models with 17 meV axions (black dotted line).

will be discussed next.

In Figure 14 it is shown an axion-less sequence of $M_{WD} = 0.537M_{\odot}$ and $Z = 0.004$, and its counterpart with 17meV axions. The beginning of the cooling is indistinguishable for both sequences, but the occurrence of a subflash in the sequence with axions makes them different. The sub-flashes are observed to occur for the axion-less lowest mass sequences [3, 4]. However, when the emission of axions is considered, the mass limit to the occurrence of sub-flashes increases. It seems therefore that the axion emission is causing these sequences to experience the sub-flash. The sequences that present a sub-flash at the beginning of the cooling are marked with an asterisk at Table 1.

The sub flashes happen as a consequence of an increase in the luminosity due to shell hydrogen burning at high effective temperatures [3]. When the star enters the cooling sequence, the temperatures are still high enough for the residual nuclear reactions to be non-negligible. For the low mass sequences, in which the thicker envelope causes the pressure to be higher in the hydrogen-burning shell, these instabilities can lead to a sub-flash. The manifestation of the sub flashes in sequences with axions was not yet found to be investigated in the literature. I understand that when the axions are included in the models, the central temperature of the white dwarf drops, and to maintain the equilibrium the core shrinks. Half of the energy is then released in the form of thermal energy (Virial theorem). This energy heats the upper layers and therefore increases the hydrogen burning rate. The sub-flashes take place during a short period of time (∼kyrs) that is negligible

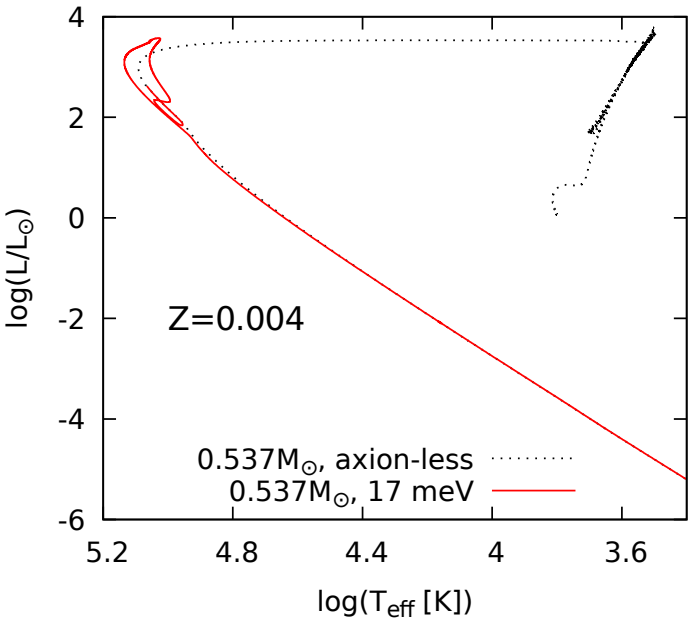

Figure 14 – Hertzprung-Russell diagram of the evolutionary sequences of $0.537M_{\odot}$ for Z= 0.004. The dotted black line is the full sequence without axions [3], and the continuous red line is the cooling sequence of the 17 meV axions sequence that experiences a sub-flash at the beginning of the cooling.

considering the timescales of the white dwarf cooling. For this reason, the sub-flashes do not have an impact on the age of white dwarfs. Since hydrogen is consumed during the sub-flashes, the hydrogen content could be affected. However, in my analysis, I did not find a significant difference in the hydrogen amount for sequences with and without sub-flashes.

I also analysed the impact of axions into two processes that take place in white dwarfs at low temperatures ($T_{\rm eff} \lesssim 10\,000$K): crystallization [76] and convective coupling [4]. Both processes are considered in my models and none of them is affected by the inclusion of axions.

4.1.4 Cooling rate

In Figure 15 I plot the cooling rate of white dwarfs models of 0.570 and $0.817M_{\odot}$, $Z = 0.01$ as a function of the effective temperature. I show the models including 17 and 30 meV axions, as well as the axion-less model. The cooling rate of models including axions is shown to be several times larger than the cooling rate of axion-less models. For the $0.570M_{\odot}$ sequence, the cooling rate including 30 meV axions achieve $\sim 5\times$ the cooling rate of the axion-less model, while for the $0.877M_{\odot}$ sequence the cooling rate can increase by a factor of ~ 9 at high effective temperatures. I conclude that the emission of axions severely affects the cooling rate of white dwarfs, mainly the more massive ones. Additionally, it can be seen that the axions will have an impact on the cooling rate of white dwarfs depending on how massive the axions are.

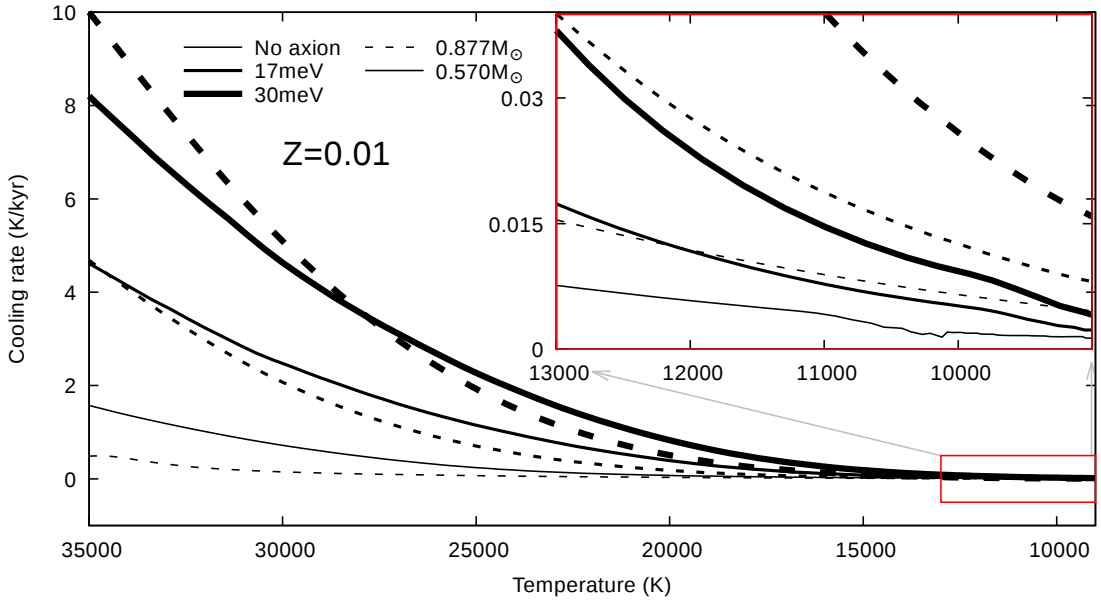

Figure 15 – The cooling rate in function of effective temperature for Z=0.01 models without axions and with axions of 17 and 30meV (thicker line for higher axion mass). Two white dwarf masses are shown: $M = 0.570 M_{\odot}$ (dashed lines) and $M = 0.877 M_{\odot}$ (continuous lines). The zoom embraces the temperature range in which we can find pulsating white dwarfs with the cooling rate determined.

The cooling rate of white dwarfs is a property that can be indirectly measured by observation of the variation of the periods of a pulsating white dwarf ($\frac{dP}{dt}$). For hydrogen-rich atmosphere white dwarfs, pulsations are present between $\sim$ 12 500 K and 10 500 K [79]. In this region, highlighted in figure 15, the cooling rate of white dwarfs of different masses is increased by the same factor ($\sim 2\times$ for 17 meV axions). The increase in the cooling speed is still large enough to be measurable using pulsating white dwarfs. I found no favored mass to test the cooling rate of white dwarfs in this temperature range, as for all the cooling rate are increased by the same magnitude.

In Figure 16 I show the age difference between axion-less models and models including axions at fixed effective temperatures. The age difference is caused by the increase of the cooling rate by axions. I note that the age difference is larger for models including 30 meV axions than for models including 17 meV axions. It indicates that more massive axions would have a higher impact on the ages of white dwarf stars. It is an expected result since more massive axions can take more energy away from the star than lower mass ones.

The age difference between axion-less models and models including axions shown in figure 16 reach several Gyrs at low effective temperatures ($< 6\,000$ K). For 17 meV axions the age difference reaches more than 2 Gyr at temperatures lower than 5 000 K,

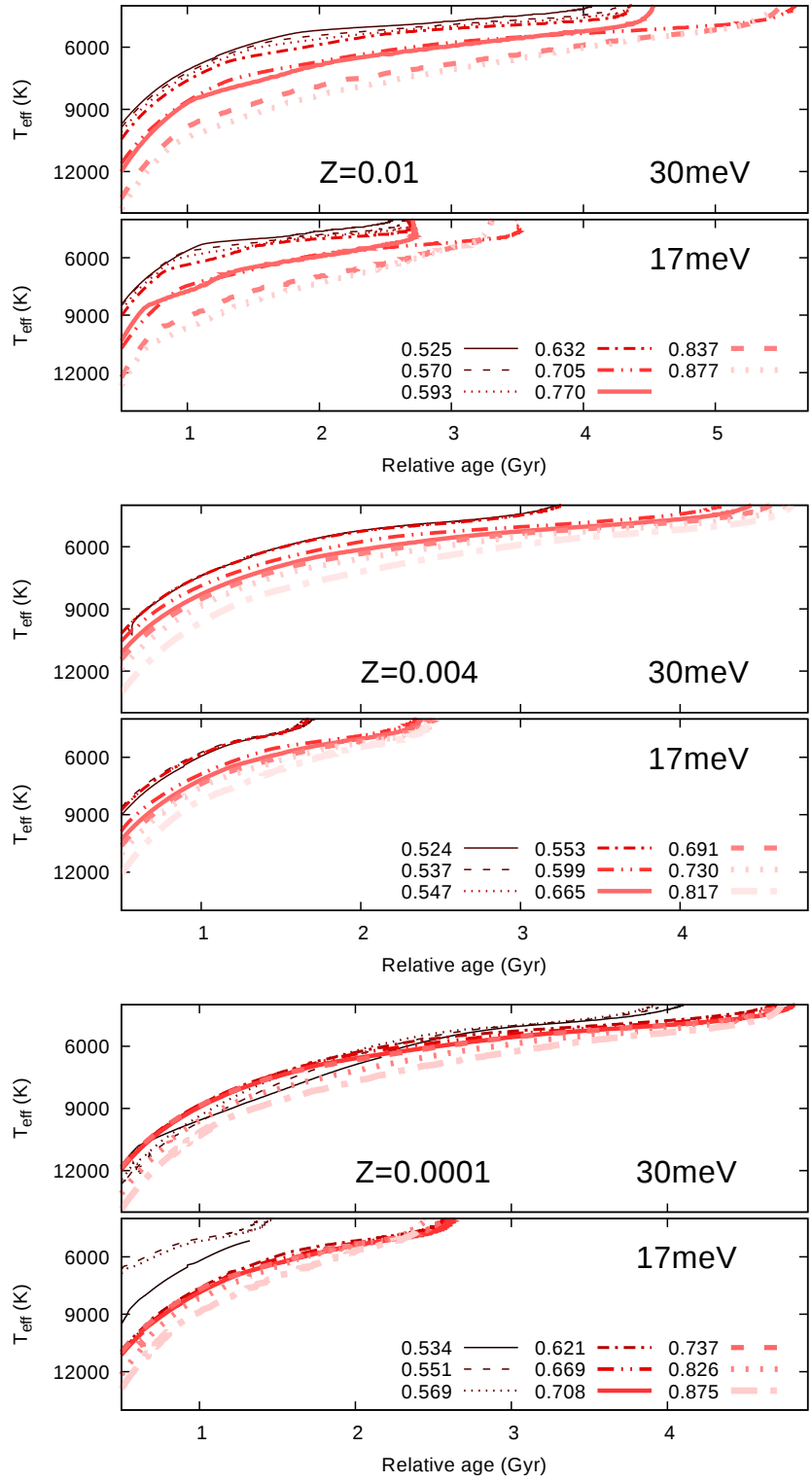

Figure 16 – Age difference for models with and without axions at the same effective temperature (Age_0-$\mathrm{Age}_{17/30meV}$ at fixed T_{eff}) against the effective temperature of the models. The upper panel shows the age difference for the $Z = 0.01$ models, the middle one for $Z = 0.004$, and the bottom one for $Z = 0.0001$. For each plot, the upper panel shows the age difference between models with axions of 30 meV and the models without axions, while the bottom one shows the age difference between models with axions of 17 meV and the models without axions. Each line represents one white dwarf mass, with legends on the figure.

while for 30 meV axions the difference can reach more than 5 Gyr. For a typical white dwarf ($\sim 0.6 M_{\odot}$) I estimate the impact of axions in age as being $\sim 25\%$ for temperatures between 10 000 K and 4 000 K. The impact on the total age is, however, more severe for more massive white dwarfs, once they spend a larger fraction of their evolution on the cooling sequence when compared to lower mass ones. In addition, the more massive a white dwarf is, the greater the impact of axions in the cooling rate (see figure 15).

I show in figure 16 the age difference for more than one metallicity. The age difference caused by axions is similar between different metallicity models. The impact of axions on the age seems to be mostly independent of the metallicity.

4.1.5 Isochrones

In Figure 17 I show isochrones for models with initial metallicity of Z=0.01 and a total age of 12 Gyrs. I present three isochrones: (i) without axion emission and considering the emission of axions with (ii) 17 and (iii) 30 meV. The three isochrones present a blue turn, which is a turn to higher temperatures caused by the mass spread. The blue turn of the axion-less isochrone, however, occurs at $log(L) \approx -4.5$, while the ones including axions occur at lower luminosities. As the blue turn is one of the features used to determine the age of globular clusters [1], [80], [2], [81], the change in its position in the CMD due to axions can be a powerful tool to constrain the axion mass.

In this work I used the Z=0.004 isochrones to test the difference in the age determination of the globular cluster 47 Tucanae between models with and without axions. To simulate the white dwarf population of 47 Tucanae, I employ the population sunthesis code described in section 3.1.2. For the distance modulus, reddening and the initial-to-final mass function I used the values determined by Campos, F. in 2016 [2]: $\mu_0 = 13.28$, $A_V = 0.14$ and $\alpha = 3.42$.

I generated simulated CMDs for 47 Tucanae using models without and including 17 and 30 meV axions, spanning ages from 6 to 12 Gyr. I compared my simulations with the photometric data of the white dwarf stars of the globular cluster 47 Tucanae. The data was obtained with the ACS camera of the Hubble Space Telescope (HST) (GO-11677, PI: H. Richer).

The observed data and the simulations that best fit the observed CMD for 47 Tucanae are presented in Fig 18. On the left panel I show the proper-motion cleaned data. The second panel shows my simulation for axion-less models that fits the observation the best, and the third and fourth ones show the simulations that fits the observation the best with models including axions of 17 meV and 30 meV, respectively.

The best fit I found using the axion-less models was for age $= 11.0 \pm 0.9$Gyr. This value is consistent with the Campos, F. (2016) [2] work (age$=10.95^{+0.21}_{-0.15}$Gyr). For the

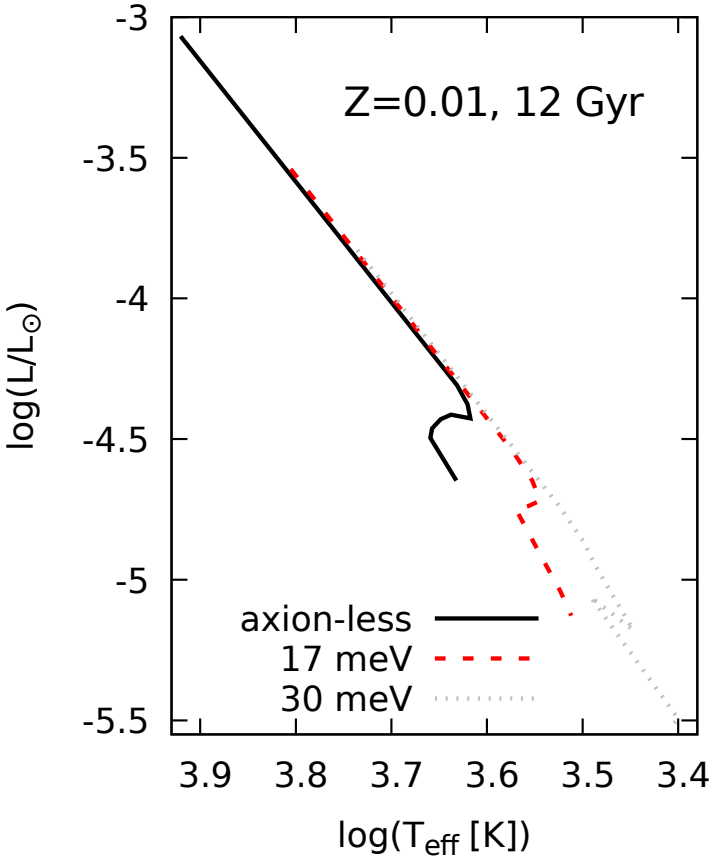

Figure 17 – Isochrones of 12Gyr for Z=0.01 using axion-less models, (black continuous line), with 17meV axions (red dashed line) and with 30meV axions (gray dotted line).

simulation including 17 meV axions, the minimum χ^2 was obtained for age$= 8.9 \pm 1.2$Gyr, while for 30 meV the minimum χ^2 was for age$= 6.8 \pm 1.0$Gyr.

The simulation using 17 meV axions sequences reproduced the blue turn at the same luminosity as in the data. The number of stars in each region of the color-magnitude diagram was also approximately reproduced. The necessary age for the simulation to reproduce the data is, however, significantly lower than the ages determined by other methods for 47 Tucanae.

The usage of main-sequence stars to determine the age of a globular cluster should not be considerably impacted by the existence of axions, thus providing an independent measure to compare with. The most recent studies using the main-sequence stars to set an age for 47 Tucanae resulted in age$=12.8 - 13.1(\pm 1.5)$ Gyr [82], $11.8 Gyr^{+1.6}_{-1.4}$ [83], 11.6 ± 0.7 [84]. For the 1 sigma analysis, the age determined for 47 Tuc using models including 17 meV axions is incompatible with the age determinations using the main sequence stars. Still, the 17 meV axion is not ruled out. For a more conservative analysis, using 3 sigma, the age for 47 Tucanae determined with 17 meV axions is 8.90 ± 3.0Gyr, which is compatible

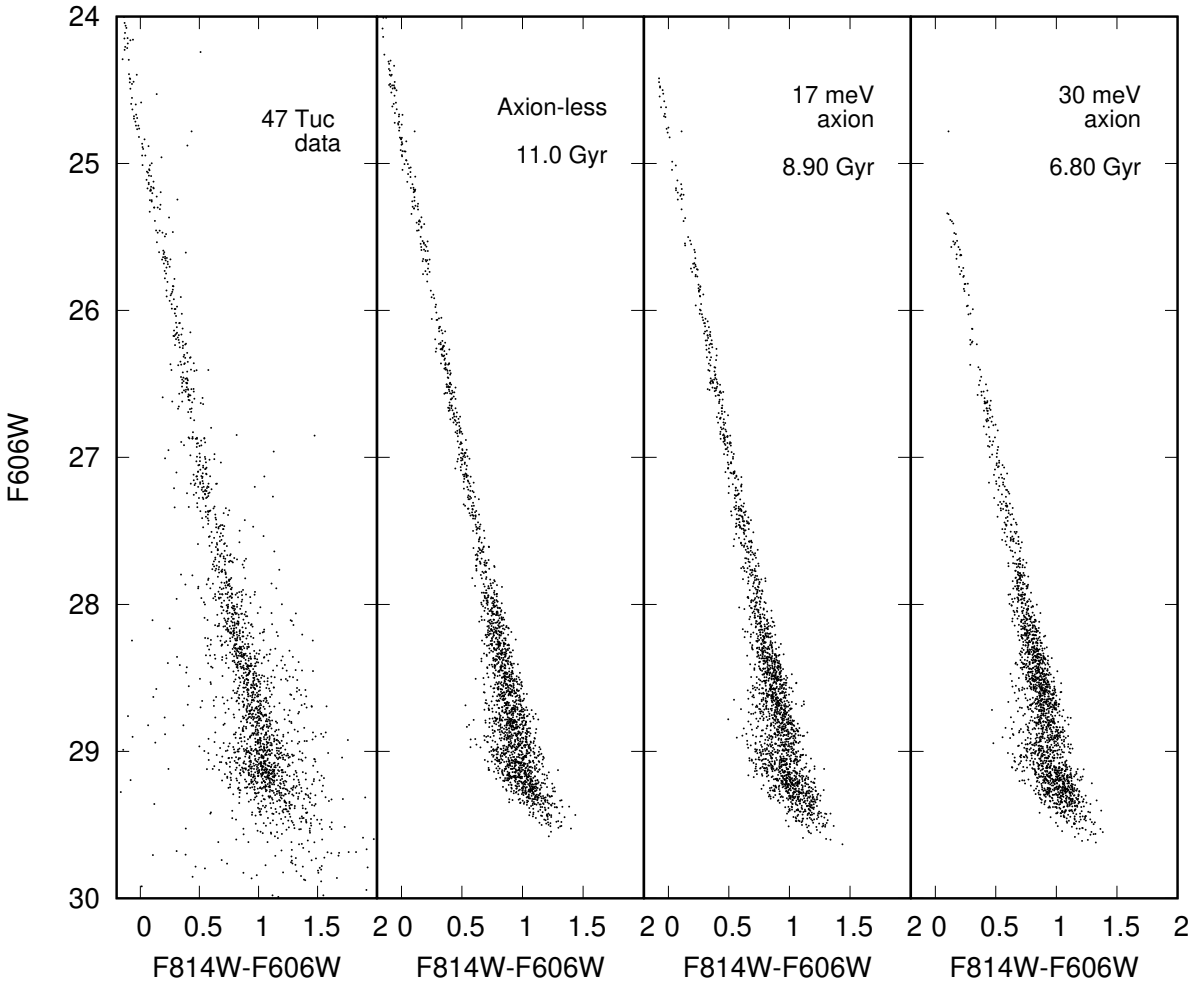

Figure 18 – 47 Tucanae proper-motion cleaned data on the left. The second panel shows the best axion-less simulation - 11 Gyr, the third one shows the best simulations with models including axions of 17 meV - 8.9 Gyr, and the fourth panel exemplifies a simulation with models including 30 meV axions - 6.8 Gyr.

with the main sequence ages.

For the 30 meV axion simulation the number of stars in each region of the color-magnitude diagram is not reproduced. Also, the determined age for 47 Tucanae using the 30 meV sequences is incompatible with other independent age determinations for the same cluster, even considering 3 sigma. The existence of such an axion is, therefore, very unlikely.

4.2 Constrains on the axion-electron coupling

Many attempts have been made to constrain the axion-electron coupling so far. The constraints on it come from the observation of several objects and using different techniques. On Figure 19 I present up to date bounds on the axion-electron coupling from

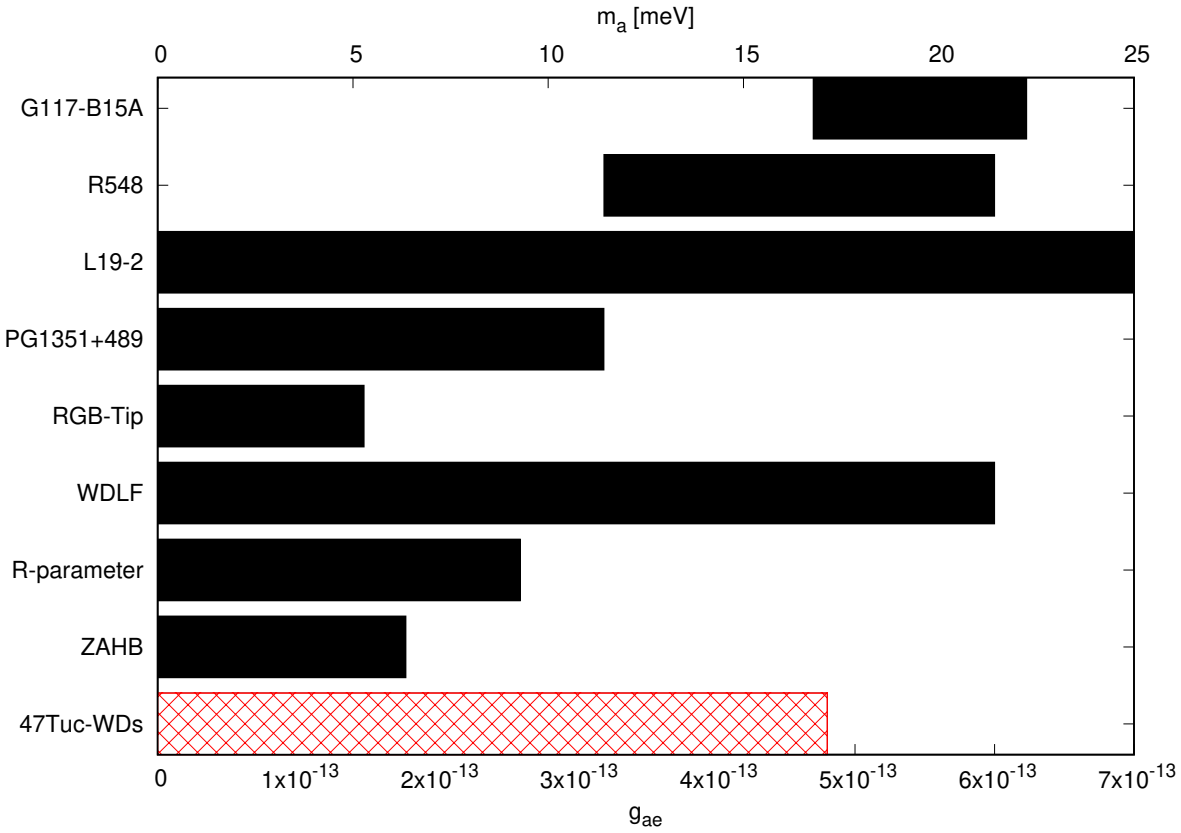

Figure 19 – Present stellar constrains on axion-electron coupling. Filled regions are the allowed by the analysis of the object on the left. Red/hatched region represents the bound I was able to determine in this paper by the 1 sigma comparison with the main-sequence ages for 47 Tuc.

stellar observations - zero age horizontal branch (ZAHB) [85], R-parameter [85], white dwarf luminosity function [56], RGB-Tip [86] and pulsating white dwarfs [58, 59, 60, 61].

In this work I present a new method to constrain this coupling, using the white dwarf cooling sequence of a globular cluster. Although the method does not allow a constrain on the axion coupling by itself, the age determined by the cluster using models with axions can be compared to other age determinations that are not affected by the presence of axions. As the age I determined for 47 Tucanae with 17 meV models and the age determinations by the main-sequence do not agree in a 1 sigma analysis, I conclude the electron-axion coupling strength should not be higher than 4.8×10^{-13}. This constrain is shown in Figure 19.

These findings may be somewhat limited by the small sample of axion masses applied on it. Further research should be undertaken to investigate the impact of axions on the globular cluster cooling sequences in order to get a more rigorous result. Yet the finding of how much the axions can alter the age of globular clusters is promising.

5 Discussion and conclusions

In this work I present consistent calculated white dwarf cooling sequence models for $Z = 0.01$, 0.004 and 0.0001 including emission of DFSZ axions with masses between 1 and 30 meV ($2.8 \times 10^{-14} < g_{ae} < 8.4 \times 10^{-13}$). My main results are linked below:

- The bremsstrahlung process is the main axion production mechanism in white dwarfs, and the Compton effect can be neglected;
- Axion emission modifies the temperature profile of the white dwarf;
- Neutrino emission is lower than in models without axions;
- Axion emission is lower than it would be expected from non consistent calculations of axion emission;
- Axions can represent the main mechanism of energy loss in white dwarf stars;
- The crystallization and convective coupling temperatures are not affected by the emission of axions;
- Emission of axions increases the residual burning rate and can lead to sub-flashes at high effective temperatures in low mass models;
- The white dwarf cooling rate can be increased by many orders due to the axion emission - depending on the axion mass. For instance, the cooling rate of models including 30meV axions can reach $\sim 9\times$ the cooling rate of axion-less models.
- The age of a cool white dwarf ($T_{\rm eff} < 3000$ K) could be overestimated by $\sim$ 2Gyrs (17 meV axions) or even $\sim$ 4Gyr (30 meV axions) if axions exist;
- All these findings were verified for three metallicities, endorsing the idea that the metallicity does not affect significantly the axion emission.

The calculations of the white dwarf cooling sequences with axions also provided tools to test the possibility of axion emission in a number of stellar systems. In this work I tested the possibility to use the sequences with axions to determine the age of the globular cluster 47 Tucanae. The age determined with sequences including axions are not in agreement with the ages determined by the main-sequence stars, thus providing a new way to constrain the axion mass.

The cooling rate of a white dwarf is, however, subject to some theoretical considerations. There are still uncertainties in the ^{22}Ne deposition, which can delay the white

dwarf cooling in billions of years [87, 88, 89]. Also the thickness of the outer layers can affect the cooling, as well of the carbon-oxygen phase separation treatment and the C/O reaction rates. In spite of its limitations, the study certainly adds to our understanding of the impact of axions in the white dwarf cooling.

The employment of stellar objects and especially white dwarf stars has been shown to be a powerful tool to test the physics beyond the standard model. During the last decades the existence of axions has been tested in several stellar systems, and the methods are improving each year. Hopefully the analysis made in this work will help to improve future studies in the subject.

Bibliography

[1] Richer, H. B.; Goldsbury, R.; Heyl, J.; Hurley, J.; Dotter, A.; Kalirai, J. S.; Woodley, K. A.; Fahlman, G. G.; Rich, R. M.; Shara, M. M. Comparing the White Dwarf Cooling Sequences in 47 Tuc and NGC 6397. , v. 778, n. 2, p. 104, Dec. 2013. Citado 3 vezes nas páginas 17, 35, and 65.

[2] Campos, F.; Bergeron, P.; Romero, A. D.; Kepler, S. O.; Ourique, G.; Costa, J. E. S.; Bonatto, C. J.; Winget, D. E.; Montgomery, M. H.; Pacheco, T. A.; Bedin, L. R. A comparative analysis of the observed white dwarf cooling sequence from globular clusters. , v. 456, n. 4, p. 3729–3742, Mar. 2016. Citado 5 vezes nas páginas 17, 50, 51, 55, and 65.

[3] Romero, A. D.; Campos, F.; Kepler, S. O. The age-metallicity dependence for white dwarf stars. , v. 450, n. 4, p. 3708–3723, July 2015. Citado 7 vezes nas páginas 18, 21, 49, 52, 55, 61, and 62.

[4] Renedo, I.; Althaus, L. G.; Miller Bertolami, M. M.; Romero, A. D.; Córsico, A. H.; Rohrmann, R. D.; García-Berro, E. New Cooling Sequences for Old White Dwarfs. , v. 717, n. 1, p. 183–195, July 2010. Citado 5 vezes nas páginas 21, 49, 51, 61, and 62.

[5] Kippenhahn, R.; Weigert, A.; Weiss, A. *Stellar Structure and Evolution*. 2012. Citado na página 29.

[6] Althaus, L. G.; Córsico, A. H.; Isern, J.; García-Berro, E. Evolutionary and pulsational properties of white dwarf stars. , v. 18, n. 4, p. 471–566, Oct. 2010. Citado 2 vezes nas páginas 32 and 51.

[7] Russell, H. N. Relations Between the Spectra and Other Characteristics of the Stars. *Popular Astronomy*, v. 22, p. 275–294, May 1914. Citado na página 32.

[8] Adams, W. S. The Spectrum of the Companion of Sirius. , v. 27, n. 161, p. 236, Dec. 1915. Citado na página 32.

[9] Fowler, R. H. On dense matter. , v. 87, p. 114–122, Dec. 1926. Citado na página 32.

[10] Lauffer, G. R.; Romero, A. D.; Kepler, S. O. New full evolutionary sequences of H- and He-atmosphere massive white dwarf stars using MESA. , v. 480, n. 2, p. 1547–1562, Oct. 2018. Citado na página 33.

[11] Salpeter, E. E. The Luminosity Function and Stellar Evolution. , v. 121, p. 161, Jan. 1955. Citado 2 vezes nas páginas 33 and 55.

[12] Itoh, N.; Hayashi, H.; Nishikawa, A.; Kohyama, Y. Neutrino Energy Loss in Stellar Interiors. VII. Pair, Photo-, Plasma, Bremsstrahlung, and Recombination Neutrino Processes. , v. 102, p. 411, Feb. 1996. Citado 2 vezes nas páginas 33 and 53.

[13] Miller Bertolami, M. M.; Melendez, B. E.; Althaus, L. G.; Isern, J. Revisiting the axion bounds from the Galactic white dwarf luminosity function. , v. 2014, n. 10, p. 069, Oct. 2014. Citado 3 vezes nas páginas 33, 51, and 60.

[14] van Horn, H. M. Crystallization of White Dwarfs. , v. 151, p. 227, Jan. 1968. Citado na página 34.

[15] BERTONE, G.; HOOPER, D. History of dark matter. *Reviews of Modern Physics*, Woodbury, v. 90, n. 4, Oct 2018. Citado na página 36.

[16] Zwicky, F. Die Rotverschiebung von extragalaktischen Nebeln. *Helvetica Physica Acta*, Basel, v. 6, p. 110–127, Jan. 1933. Citado 2 vezes nas páginas 36 and 37.

[17] Smith, S. The Mass of the Virgo Cluster. , v. 83, p. 23, Jan. 1936. Citado na página 36.

[18] Rubin, V. C.; Ford, W. KENT, J. Rotation of the Andromeda Nebula from a Spectroscopic Survey of Emission Regions. , v. 159, p. 379, Feb. 1970. Citado na página 36.

[19] Roberts, M. S. A High-Resolution 21-CM Hydrogen-Line Survey of the Andromeda Nebula. , v. 144, p. 639, May 1966. Citado na página 36.

[20] Freeman, K. C. On the Disks of Spiral and S0 Galaxies. , v. 160, p. 811, June 1970. Citado na página 36.

[21] NAVARRO, J. F.; FRENK, C. S.; WHITE, S. D. M. A universal density profile from hierarchical clustering. *The Astrophysical Journal*, v. 490, n. 2, p. 493–508, Dec 1997. Citado na página 37.

[22] Harvey, D.; Massey, R.; Kitching, T.; Taylor, A.; Tittley, E. The nongravitational interactions of dark matter in colliding galaxy clusters. *Science*, Washington, v. 347, n. 6229, p. 1462–1465, Mar. 2015. Citado na página 40.

[23] Taoso, M.; Bertone, G.; Masiero, A. Dark matter candidates: a ten-point test. , v. 2008, n. 3, p. 022, Mar. 2008. Citado na página 41.

[24] BRANDT, T. D. Constraints on macho dark matter from compact stellar systems in ultra-faint dwarf galaxies. *The Astrophysical Journal*, v. 824, n. 2, p. L31, Jun 2016. Citado na página 42.

[25] WILCZEK, F. Problem of strong p and t invariance in the presence of instantons. *Phys. Rev. Lett.*, v. 40, p. 279–282, Jan 1978. Citado na página 43.

[26] WEINBERG, S. A new light boson? *Phys. Rev. Lett.*, v. 40, p. 223–226, Jan 1978. Citado 2 vezes nas páginas 43 and 44.

[27] PECCEI, R. D.; QUINN, H. R. CP conservation in the presence of pseudoparticles. *Phys. Rev. Lett.*, v. 38, p. 1440–1443, Jun 1977. Citado 2 vezes nas páginas 43 and 44.

[28] IPSER, J.; SIKIVIE, P. Can galactic halos be made of axions? *Phys. Rev. Lett.*, v. 50, p. 925–927, Mar 1983. Citado 2 vezes nas páginas 43 and 44.

[29] Brandenberger, R. H. Quantum field theory methods and inflationary universe models. *Reviews of Modern Physics*, Woodbury, v. 57, n. 1, p. 1–60, Jan. 1985. Citado na página 43.

[30] Preskill, J.; Wise, M. B.; Wilczek, F. Cosmology of the invisible axion. *Physics Letters B*, Amsterdam, v. 120, n. 1-3, p. 127–132, Jan. 1983. Citado na página 44.

[31] Abbott, L. F.; Sikivie, P. A cosmological bound on the invisible axion. *Physics Letters B*, Amsterdam, v. 120, n. 1-3, p. 133–136, Jan. 1983. Citado na página 44.

[32] Dine, M.; Fischler, W. The not-so-harmless axion. *Physics Letters B*, Amsterdam, v. 120, n. 1-3, p. 137–141, Jan. 1983. Citado na página 44.

[33] Raffelt, G. G. Astrophysical methods to constrain axions and other novel particle phenomena. , v. 198, n. 1-2, p. 1–113, Dec. 1990. Citado na página 44.

[34] Duffy, L. D.; van Bibber, K. Axions as dark matter particles. *New Journal of Physics*, v. 11, n. 10, p. 105008, Oct. 2009. Citado na página 44.

[35] Chadha-Day, F.; Ellis, J.; Marsh, D. J. E. Axion Dark Matter: What is it and Why Now? *arXiv e-prints*, p. arXiv:2105.01406, May 2021. Citado na página 44.

[36] Sikivie, P. Invisible axion search methods. *Reviews of Modern Physics*, Woodbury, v. 93, n. 1, p. 015004, Jan. 2021. Citado na página 44.

[37] Gorghetto, M.; Villadoro, G. Topological susceptibility and QCD axion mass: QED and NNLO corrections. *Journal of High Energy Physics*, v. 2019, n. 3, p. 33, Mar. 2019. Citado na página 44.

[38] KIM, J. E. Weak-interaction singlet and strong CP invariance. *Phys. Rev. Lett.*, v. 43, p. 103–107, Jul 1979. Citado na página 44.

[39] SHIFMAN, M.; VAINSHTEIN, A.; ZAKHAROV, V. Can confinement ensure natural cp invariance of strong interactions? *Nuclear Physics B*, Amsterdam, v. 166, n. 3, p. 493–506, 4 1980. Citado na página 44.

[40] DINE, M.; FISCHLER, W.; SREDNICKI, M. A simple solution to the strong cp problem with a harmless axion. *Physics Letters, Section B: Nuclear, Elementary Particle and High-Energy Physics*, v. 104, n. 3, p. 199–202, 8 1981. Citado na página 44.

[41] ZHITNITSKY, A. R. On Possible Suppression of the Axion Hadron Interactions. (In Russian). *Sov. J. Nucl. Phys.*, v. 31, p. 260, 1980. [Yad. Fiz.31,497(1980)]. Citado na página 44.

[42] di Cortona, G. G.; Hardy, E.; Vega, J. P.; Villadoro, G. The QCD axion, precisely. *Journal of High Energy Physics*, v. 2016, p. 34, Jan. 2016. Citado na página 45.

[43] Raffelt, G. G. *Stars as laboratories for fundamental physics : the astrophysics of neutrinos, axions, and other weakly interacting particles*. 1996. Citado 2 vezes nas páginas 45 and 54.

[44] OUELLET, J. L.; SALEMI, C. P.; FOSTER, J. W.; HENNING, R.; BOGORAD, Z.; CONRAD, J. M.; FORMAGGIO, J. A.; KAHN, Y.; MINERVINI, J.; RADOVINSKY, A.; ET AL. First results from abracadabra-10 cm: A search for sub- ev axion dark matter. *Physical Review Letters*, Woodbury, v. 122, n. 12, Mar 2019. Citado na página 45.

[45] DU, N.; FORCE, N.; KHATIWADA, R.; LENTZ, E.; OTTENS, R.; ROSENBERG, L. J.; RYBKA, G.; CAROSI, G.; WOOLLETT, N.; BOWRING, D.; CHOU, A. S.; SONNENSCHEIN, A.; WESTER, W.; BOUTAN, C.; OBLATH, N. S.; BRADLEY, R.; DAW, E. J.; DIXIT, A. V.; CLARKE, J.; O'KELLEY, S. R.; CRISOSTO, N.; GLEASON, J. R.; JOIS, S.; SIKIVIE, P.; STERN, I.; SULLIVAN, N. S.; TANNER, D. B.; HILTON, G. C. Search for invisible axion dark matter with the axion dark matter experiment. *Phys. Rev. Lett.*, v. 120, p. 151301, Apr 2018. Citado na página 45.

[46] CALDWELL, A.; DVALI, G.; MAJOROVITS, B.; MILLAR, A.; RAFFELT, G.; REDONDO, J.; REIMANN, O.; SIMON, F.; STEFFEN, F. Dielectric haloscopes: A new way to detect axion dark matter. *Physical Review Letters*, Woodbury, v. 118, n. 9, Mar 2017. Citado na página 45.

[47] ANASTASSOPOULOS, V. et al. New CAST Limit on the Axion-Photon Interaction. *Nature Phys.*, v. 13, p. 584–590, 2017. Citado na página 45.

[48] Raffelt, G. G. Astrophysics probes of particle physics. , v. 333, p. 593–618, Aug. 2000. Citado na página 45.

[49] Turner, M. S. Windows on the axion. , v. 197, n. 2, p. 67–97, Dec. 1990. Citado na página 45.

[50] Raffelt, G. G. *Astrophysical Axion Bounds*. 2008. v. 741, p. 51. Citado na página 45.

[51] Vinyoles, N.; Serenelli, A.; Villante, F. L.; Basu, S.; Redondo, J.; Isern, J. New axion and hidden photon constraints from a solar data global fit. , v. 2015, n. 10, p. 015, Oct. 2015. Citado na página 45.

[52] Gondolo, P.; Raffelt, G. G. Solar neutrino limit on axions and keV-mass bosons. , v. 79, n. 10, p. 107301, May 2009. Citado na página 45.

[53] Ayala, A.; Domínguez, I.; Giannotti, M.; Mirizzi, A.; Straniero, O. Revisiting the Bound on Axion-Photon Coupling from Globular Clusters. , v. 113, n. 19, p. 191302, Nov. 2014. Citado na página 45.

[54] Raffelt, G. G.; Redondo, J.; Maira, N. V. The meV mass frontier of axion physics. , v. 84, n. 10, p. 103008, Nov. 2011. Citado na página 45.

[55] Raffelt, G. G. Axion constraints from white dwarf cooling times. *Physics Letters B*, Amsterdam, v. 166, n. 4, p. 402–406, Jan. 1986. Citado na página 46.

[56] Isern, J.; García-Berro, E.; Torres, S.; Cojocaru, R.; Catalán, S. Axions and the luminosity function of white dwarfs: the thin and thick discs, and the halo. , v. 478, n. 2, p. 2569–2575, Aug 2018. Citado 2 vezes nas páginas 46 and 68.

[57] Isern, J.; Hernanz, M.; Garcia-Berro, E. Axion Cooling of White Dwarfs. , v. 392, p. L23, June 1992. Citado na página 46.

[58] Battich, T.; Córsico, A. H.; Althaus, L. G.; Miller Bertolami, M. M. First axion bounds from a pulsating helium-rich white dwarf star. , v. 2016, n. 8, p. 062, Aug. 2016. Citado 2 vezes nas páginas 46 and 68.

[59] Córsico, A. H.; Romero, A. D.; Althaus, L. D. G.; García-Berro, E.; Isern, J.; Kepler, S. O.; Miller Bertolami, M. M.; Sullivan, D. J.; Chote, P. An asteroseismic constraint on the mass of the axion from the period drift of the pulsating DA white dwarf star L19-2. , v. 2016, n. 7, p. 036, July 2016. Citado 3 vezes nas páginas 46, 51, and 68.

[60] Córsico, A. H.; Althaus, L. G.; Romero, A. D.; Mukadam, A. S.; García-Berro, E.; Isern, J.; Kepler, S. O.; Corti, M. A. An independent limit on the axion mass from the variable white dwarf star R548. , v. 2012, n. 12, p. 010, Dec. 2012. Citado 3 vezes nas páginas 46, 51, and 68.

[61] Kepler, S. O.; Winget, D. E.; Vanderbosch, Z. P.; Castanheira, B. G.; Hermes, J. J.; Bell, K. J.; Mullally, F.; Romero, A. D.; Montgomery, M. H.; DeGennaro, S.; Winget, K. I.; Chandler, D.; Jeffery, E. J.; Fritzen, J. K.; Williams, K. A.; Chote, P.; Zola, S. The Pulsating White Dwarf G117-B15A: Still the Most Stable Optical Clock Known. , v. 906, n. 1, p. 7, Jan. 2021. Citado 2 vezes nas páginas 46 and 68.

[62] Moehler, S.; Bono, G. White Dwarfs in Globular Clusters. *arXiv e-prints*, p. arXiv:0806.4456, June 2008. Citado na página 47.

[63] Althaus, L. G.; Serenelli, A. M.; Panei, J. A.; Córsico, A. H.; García-Berro, E.; Scóccola, C. G. The formation and evolution of hydrogen-deficient post-AGB white dwarfs: The emerging chemical profile and the expectations for the PG 1159-DB-DQ evolutionary connection. , v. 435, n. 2, p. 631–648, May 2005. Citado na página 51.

[64] Romero, A. D.; Kepler, S. O.; Córsico, A. H.; Althaus, L. G.; Fraga, L. Asteroseismological Study of Massive ZZ Ceti Stars with Fully Evolutionary Models. , v. 779, n. 1, p. 58, Dec. 2013. Citado na página 51.

[65] García-Berro, E.; Torres, S.; Althaus, L. R. G.; Renedo, I.; Lorén-Aguilar, P.; Córsico, A. H.; Rohrmann, R. D.; Salaris, M.; Isern, J. A white dwarf cooling age of 8Gyr for NGC 6791 from physical separation processes. , v. 465, n. 7295, p. 194–196, May 2010. Citado na página 51.

[66] Córsico, A. H.; Althaus, L. G.; Miller Bertolami, M. M.; Romero, A. D.; García-Berro, E.; Isern, J.; Kepler, S. O. The rate of cooling of the pulsating white dwarf star G117-B15A: a new asteroseismological inference of the axion mass. , v. 424, n. 4, p. 2792–2799, Aug. 2012. Citado na página 51.

[67] Magni, G.; Mazzitelli, I. Thermodynamic properties and equations of state for hydrogen and helium in stellar conditions. , v. 72, n. 1-2, p. 134–147, Feb. 1979. Citado na página 52.

[68] Caughlan, G. R.; Fowler, W. A. Thermonuclear Reaction Rates V. *Atomic Data and Nuclear Data Tables*, v. 40, p. 283, Jan. 1988. Citado na página 52.

[69] Salaris, M.; Domínguez, I.; García-Berro, E.; Hernanz, M.; Isern, J.; Mochkovitch, R. The Cooling of CO White Dwarfs: Influence of the Internal Chemical Distribution. , v. 486, n. 1, p. 413–419, Sept. 1997. Citado na página 53.

[70] Burgers, J. M. *Flow Equations for Composite Gases*. 1969. Citado na página 53.

[71] Althaus, L. G.; Serenelli, A. M.; Córsico, A. H.; Montgomery, M. H. New evolutionary models for massive ZZ Ceti stars. I. First results for their pulsational properties. , v. 404, p. 593–609, June 2003. Citado na página 53.

[72] Iglesias, C. A.; Rogers, F. J. Updated Opal Opacities. , v. 464, p. 943, June 1996. Citado na página 53.

[73] Marigo, P.; Aringer, B. Low-temperature gas opacity. ÆSOPUS: a versatile and quick computational tool. , v. 508, n. 3, p. 1539–1569, Dec. 2009. Citado na página 53.

[74] Tassoul, M.; Fontaine, G.; Winget, D. E. Evolutionary Models for Pulsation Studies of White Dwarfs. , v. 72, p. 335, Feb. 1990. Citado na página 53.

[75] Haft, M.; Raffelt, G.; Weiss, A. Standard and Nonstandard Plasma Neutrino Emission Revisited. , v. 425, p. 222, Apr. 1994. Citado na página 53.

[76] Horowitz, C. J.; Schneider, A. S.; Berry, D. K. Crystallization of Carbon-Oxygen Mixtures in White Dwarf Stars. , v. 104, n. 23, p. 231101, June 2010. Citado 2 vezes nas páginas 53 and 62.

[77] Raffelt, G.; Weiss, A. Red giant bound on the axion-electron coupling reexamined. , v. 51, n. 4, p. 1495–1498, Feb. 1995. Citado 2 vezes nas páginas 53 and 54.

[78] Nakagawa, M.; Kohyama, Y.; Itoh, N. Axion Bremsstrahlung in Dense Stars. , v. 322, p. 291, Nov. 1987. Citado na página 54.

[79] Romero, A. D.; Amaral, L. A.; Klippel, T.; Sanmartim, D.; Fraga, L.; Ourique, G.; Pelisoli, I.; Lauffer, G. R.; Kepler, S. O.; Koester, D. Ground-based observation of ZZ Ceti stars and the discovery of four new variables. , v. 490, n. 2, p. 1803–1820, Dec. 2019. Citado na página 63.

[80] Hansen, B. M. S.; Anderson, J.; Brewer, J.; Dotter, A.; Fahlman, G. G.; Hurley, J.; Kalirai, J.; King, I.; Reitzel, D.; Richer, H. B.; Rich, R. M.; Shara, M. M.; Stetson, P. B. The White Dwarf Cooling Sequence of NGC 6397. , v. 671, n. 1, p. 380–401, Dec. 2007. Citado na página 65.

[81] Torres, S.; García-Berro, E.; Althaus, L. G.; Camisassa, M. E. The white dwarf population of NGC 6397. , v. 581, p. A90, Sept. 2015. Citado na página 65.

[82] Saracino, S.; Dalessandro, E.; Ferraro, F. R.; Lanzoni, B.; Origlia, L.; Salaris, M.; Pietrinferni, A.; Geisler, D.; Kalirai, J. S.; Correnti, M.; Cohen, R. E.; Mauro, F.; Villanova, S.; Moni Bidin, C. On the Use of the Main-sequence Knee (Saddle) to Measure Globular Cluster Ages. , v. 860, n. 2, p. 95, June 2018. Citado na página 66.

[83] Brogaard, K.; VandenBerg, D. A.; Bedin, L. R.; Milone, A. P.; Thygesen, A.; Grundahl, F. The age of 47 Tuc from self-consistent isochrone fits to colour-magnitude diagrams and the eclipsing member V69. , v. 468, n. 1, p. 645–661, June 2017. Citado na página 66.

[84] Correnti, M.; Gennaro, M.; Kalirai, J. S.; Brown, T. M.; Calamida, A. Constraining Globular Cluster Age Uncertainties using the IR Color-Magnitude Diagram. , v. 823, n. 1, p. 18, May 2016. Citado na página 66.

[85] Straniero, O.; Dominguez, I.; Giannotti, M.; Mirizzi, A. Axion-electron coupling from the RGB tip of Globular Clusters. *arXiv e-prints*, p. arXiv:1802.10357, Feb. 2018. Citado na página 68.

[86] Straniero, O.; Pallanca, C.; Dalessandro, E.; Domínguez, I.; Ferraro, F. R.; Giannotti, M.; Mirizzi, A.; Piersanti, L. The RGB tip of galactic globular clusters and the revision of the axion-electron coupling bound. , v. 644, p. A166, Dec. 2020. Citado na página 68.

[87] Bauer, E. B.; Schwab, J.; Bildsten, L.; Cheng, S. Multi-gigayear White Dwarf Cooling Delays from Clustering-enhanced Gravitational Sedimentation. , v. 902, n. 2, p. 93, Oct. 2020. Citado na página 70.

[88] Camisassa, M. E.; Althaus, L. G.; Córsico, A. H.; Vinyoles, N.; Serenelli, A. M.; Isern, J.; Miller Bertolami, M. M.; García–Berro, E. The Effect of ^{22}NE Diffusion in the Evolution and Pulsational Properties of White Dwarfs with Solar Metallicity Progenitors. , v. 823, n. 2, p. 158, June 2016. Citado na página 70.

[89] Tononi, J.; Torres, S.; García-Berro, E.; Camisassa, M. E.; Althaus, L. G.; Rebassa-Mansergas, A. Effects of ^{22}Ne sedimentation and metallicity on the local 40 pc white dwarf luminosity function. , v. 628, p. A52, Aug. 2019. Citado na página 70.